Process Biochemistry 64 (2018) 177–192

Contents lists available at ScienceDirect

Process Biochemistry

journal homepage: www.elsevier.com/locate/procbio

# Structural and functional stabilization of bacteriophage particles within the aqueous core of a W/O/W multiple emulsion: A potential biotherapeutic system for the inhalational treatment of bacterial pneumonia

Alessandra C. Rios[a], Marta M.D.C. Vila[a], Renata Lima[a], Fernando S. Del Fiol[a], Matthieu Tubino[b], José A. Teixeira[c], Victor M. Balcão[a,c,*]

[a] PhageLab—Laboratory of Biofilms and Bacteriophages of UNISO, i(bs)2—Intelligent Biosensing and Biomolecule Stabilization Research Group, University of Sorocaba, Sorocaba, SP, Brazil
[b] Institute of Chemistry, University of Campinas, Campinas, SP, Brazil
[c] CEB—Centre of Biological Engineering, University of Minho, Braga, Portugal

ARTICLE INFO

*Keywords:*
Aqueous-core lipid nanodroplets
Bacteriophage particles
Water-in-oil-in-water multiple emulsions
Structural and functional stabilization
Bacterial pneumonia
Inhalational phage therapy

ABSTRACT

The increase of antibiotic-resistant bacteria is growing every day, most likely associated with the indiscriminate use of these antimicrobials or even with evolutionary adaptability of bacteria to their environment. This situation brings a need to develop new alternatives to conventional antibiotics, and thus the application of strictly lytic bacteriophages has been proposed as an alternative (or complement) to the former, allowing release of the natural predators of bacteria directly where they are needed the most: the infection site. The main advantages of bacteriophages to treat infections is the maintenance of a high concentration of bacteriophage particles in the action site while any viable target bacteria still exist, coupled to the production of enzymes that hydrolyze the polymeric matrix of bacterial biofilms promoting penetration and antibacterial action. In the research effort entertained herein, the potential for protection and stabilization of strictly lytic bacteriophages with broad spectrum capable of infecting *Pseudomonas aeruginosa*, so as to maintain their structure and functionality, was investigated via encapsulation within the aqueous-core of lipid nanodroplets integrating a W/O/W multiple emulsion system, aiming at developing isotonic derivative solutions thereof for administration by nebulization.

## 1. Introduction

The increasing worldwide awareness related to the appearance of multiple bacterial resistance to conventional chemical antibiotics [1,2] has shed a renewed interest from the scientific community to bacteriophage (or phage) particles, with these inert (i.e., devoid of any metabolic machinery) entities being re-discovered as high-potential candidates for biopharmaceutical (antimicrobial) applications [3–7]. However, like most biological (macro)molecules, phage particles are intrinsically fragile and therefore their full structural and functional stabilization is mandatory [3,4,8–11] prior to any use. Solubilization of these protein-like entities in the aqueous-core of lipid nanodroplets, protecting them from deactivation by the immune system, dilution effects, and from any chemical stress [12–15], will thus promote their structural and functional stabilization [3,4,9,10], a *sine qua non* condition for these particles to be used as (bio)medicines. Colloidal systems such as water-in-oil-in-water (W/O/W) multiple emulsions (MEs) are systems in which dispersions of small water droplets within larger oil droplets are themselves dispersed in a continuous (external) aqueous phase [8,10,16–22]. The smaller the sizes of the aqueous-core lipid nanodroplets the longer their retention times [23,24], and hence such (lytic) phage-encasing nanodroplets could be utilized, e.g. in the formulation of isotonic aerosols to eliminate bacterial pneumonia caused by *Pseudomonas aeruginosa* with one clear advantage: the adhesion of these lipid nanodroplets to the pulmonary mucosa could slowly liberate their bacterial predatory content, reducing both the need for chemical antibiotics and infection elimination time. *P. aeruginosa* is the second pathogen causing nosocomial pneumonia [25,26]. Worldwide, it is found that the antimicrobial resistance rate for *P. aeruginosa* has increased dramatically [27–30]. Quite recently, a newly developed nanocontainment technique for stabilization of protein entities has started to gain momentum [8,10,31–35]. Entropic confinement (physical entrapment) of macromolecular (protein-like) entities such as phage particles within the aqueous core of these lipid nanodroplets, changes

* Corresponding author at: Universidade de Sorocaba (UNISO), Cidade Universitária Prof. Aldo Vannucchi, Rod. Raposo Tavares km 92.5, CEP 18023-000 Sorocaba, SP, São Paulo, Brazil.
*E-mail address:* victor.balcao@prof.uniso.br (V.M. Balcão).

http://dx.doi.org/10.1016/j.procbio.2017.09.022
Received 10 July 2017; Received in revised form 16 September 2017; Accepted 20 September 2017
Available online 22 September 2017
1359-5113/ 

the water activity in their microneighborhood while reducing molecular motions [9], leading to increased viscosity [9,34,36]. Lipid nanodroplets integrating a W/O/W ME are composed of a (physiologically compatible) lipid matrix [8,10,31,32,37,38], stabilized by emulsifiers such as phospholipids and/or polyoxyethylene ethers [8,10,16,31,32,39]. When producing a W/O/W ME system, the lipid concentration required to produce the lipid nanodroplets must be kept at low levels, since high lipid concentrations further enhance the thermodynamic instability of these systems and may even promote their rupture (following release of the inner aqueous core under shear rate, with concomitant expulsion of the water-soluble protein entities through the oily layer between both water phases) [16,40,41]. In the research effort entertained herein, a stable W/O/W ME system was produced according to the procedure described by Glasser et al. [8,31], integrating small-sized lipid nanodroplets with aqueous cores housing phage particles; such phage-encasing W/O/W ME was then used for developing an isotonic system aiming at the administration via nebulization for the inhalation of lytic (endotoxin-free) phages for the treatment of pulmonary infection by *P. aeruginosa*. Hence, the natural predators of bacteria responsible for provoking lung infections would be released directly where they are needed the most: the site of infection.

## 2. Materials and methods

### 2.1. Materials

#### 2.1.1. Biological materials

Bacteriophage: Bacteriophage JG004 (ref. DSM 19871) was purchased from Leibniz-Institute DSMZ (Braunschweig, Germany). Bacterial host: Phage JG004 was propagated in a *Pseudomonas aeruginosa* host (ref. DSM 19880), acquired from DSMZ. Cell lines: The cell lines were purchased from BCRJ (Duque de Caxias/RJ, Brazil): cell line V79-4 (BCRJ code 0244; Chinese Hamster, Lung-Normal); cell line A549 (BCRJ code 0033; Human, Caucasian, Lung-Carcinoma), and cell line 3T3 (BCRJ code 0017; Mus musculus (Swiss albino), Fibroblast/Embrio). Dulbecco's Modified Eagle's Medium (DMEM) was from Gibco Life Technologies (Alto de Pinheiros, São Paulo/SP, Brazil). The Tali® Apoptosis Kit (consisting of Annexin V Alexa Fluor® 488 and Propidium Iodide) was purchased from Invitrogen (Carlsbad CA, U.S.A.).

#### 2.1.2. Chemicals

***Lipids***: Softisan100™ was a kind gift from Sasol (Sasol Olefins & Surfactants GmbH, Hamburg, Germany) and glycerol was from Fluka (Steinheim, Germany). ***Surfactants***: Tween 80 was from Sigma-Aldrich (St. Louis MO, USA). Kolliphor P188™ (poloxamer 188) was a kind gift from BASF ChemTrade GmbH (Ludwigshafen, Germany). Soybean phosphatidylcholine (lecithin) was from Alamar Tecno-Científica Ltda (Diadema/SP, Brazil). ***Other chemicals***: Commercial HCl (37%, w/w) was from ECIBRA Analytical Reagents (Curitiba/PR, Brazil). Anhydrous $Na_2HPO_4$, $NaH_2PO_4$, $CaCl_2$ and NaCl were from Dinâmica Ltda (Diadema/SP, Brazil). Luria Bertani Broth (Miller, LB-Broth) was from HiMedia Laboratories Pvt. Ltd (Mumbai, India) and solid agar was from Gibco Diagnostics (Madison WI, U.S.A.). The sterilizing filtration system (Stericup™-GP, polyethersulphate (PES) membrane with 0.22 μm pore diameter) was a kind gift from Merck-Millipore (Darmstadt, Germany). Nipagin™ (methylparaben) and $MgSO_4$ were from Labsynth (Diadema/SP, Brazil). Tap water was purified in a Milli-Q Plus 185 system (Molsheim, France) to a final conductivity of ca. 18.2 $M\Omega.cm^{-1}$. MTT (3-(4,5-dimethylthiazol-2-yl)-2,5-diphenyltetrazolium bromide) and DMSO were from Sigma-Aldrich (St. Louis MO, U.S.A.).

#### 2.1.3. Analytical equipment

Zeta Potential (ZP), Hydrodynamic Size (HS) and Polydispersity Index (PI) were determined in a ZetaPALS system (model NanoBrook 90PlusPALS from Brookhaven Instruments, Holtsville NY, U.S.A.). FTIR spectra were gathered in a Fourier Transform Infrared Spectrophotometer from AGILENT (model Cary 630, Santa Clara CA, U.S.A.). X-ray diffractograms were gathered in an X-ray Diffractometer (XRD) from Shimadzu (model XRD7000, Kyoto, Japan). Nanoparticle Tracking Analyses (NTA) were carried out in a NanoSight device from Malvern Instruments Ltd (model LM14C, Worcestershire, United Kingdom), with NTA software (NanoSight version 3.1). The UV–vis Spectrophotometer was from Perkin Elmer (model Lambda 3s, Waltham MA, U.S.A). TGA analyses were carried out using a thermogravimeter from TA Instruments (model 2050, New Castle, U.S.A.), whereas DSC analyses were carried out using a differential scanning microcalorimeter from TA Instruments (model MDSC 2910, New Castle, U.S.A.). TEM analyses were carried out in a Transmission Electron Microscope from JEOL (model JEM-1400Plus, JEOL, Tokyo, Japan), equipped with a lanthanum hexaboride ($LaB_6$) filament, operating at 120 kV, and a high-resolution CCD camera from GATAN Inc. (model MultiScan 794, Pleasanton CA, U.S.A.) with a resolution of 1k x 1k pixels for the acquisition of digital images. Cell viability readings via the MTT assays were carried out in an ELISA microplate reader from Robonik India Private Ltd. (model *Readwell PLATE*, Maharashtra, India). All optical microscopy analyses for the Comet™ assays were carried out in a Zeiss Axiovert-60 optical microscope (Carl-Zeiss, Göschwitzer Str., Jena, Germany).

### 2.2. Experimental procedures

#### 2.2.1. Propagation and purification of bacteriophage JG004

The phage (JG004, ref. DSM 19871) was propagated using a specific host microorganism, namely *P. aeruginosa* (ref. DSM 19880), grown in LB molten agar.

**Preparation of a bacterial suspension of *P. aeruginosa*.** The lyophilized pellet was dissolved in 4.5 mL of Luria-Bertani Broth with the aid of a sterile loop, and 1 mL of the resulting suspension was plated on the surface of LB solid medium in Petri plates, which were then incubated during 24 h at 37 °C. For preparation of a suitable bacterial suspension, a single CFU was inoculated in a test tube containing 5 mL sterile LB-broth which was then incubated at 37 °C during 18 h.

**Propagation of the bacteriophage.** For propagation of the phage (maintained at 4 °C as a concentrated suspension), duplicate serial dilutions ($1 \times 10^{-1}$–$1 \times 10^{-10}$) (total volume of 1000 μL) in sterile phage buffer (PB) were duly prepared. To test tubes containing 4 mL LB top agar (maintained at 40 °C), 300 μL of a 1:10 dilution of the bacterial suspension in LB-broth were added together with 1000 μL of a given phage dilution. The resulting mixture was gently shaken, immediately poured and spread on top of Petri plates containing 25 mL solid Luria-Bertani agar, which were then incubated overnight at 37 °C.

**Purification of the bacteriophage.** After the incubation period, all Petri plates were visually inspected for the presence of plaque forming units (PFU) and, for those where complete lysis of the bacterial lawn occurred or where PFU's were visible, 3 mL PB solution were added to each Petri plate, after which they were isolated with Parafilm™ (to prevent them from drying out) and further incubated at room temperature during 3 h. Following this time period, the layer of top agar was fragmented by gently swirling a sterile loop, and the mixture of PB and top agar was collected into a sterile 50-mL Falcon tube. Cell debris and agar were then removed by centrifugation (5500 rpm, 15 min at 4 °C), and the supernatant carefully collected, filtered under vacuum through a sterilizing Stericup™-GP device (equipped with a PES membrane with 0.22 μm pore diameter), and stored at 4 °C until use was in order.

**Determination of bacteriophage titer.** For determination of phage concentration in the stock-suspension, the propagation procedure was repeated, with small differences, namely the plating of a top agar layer containing 100 μL of a given serial dilution of the phage stock-suspension in PB and 300 μL of the bacterial suspension. This procedure

**Table 1**
Microbiological data gathered from the PFU determination assays, allowing determination of the phage titer of concentrated bacteriophage suspension.

| Temperature (°C) | Number of PFUs | Dilution | Volume of inoculum (mL) | Phage particle concentration (PFU/mL) |
|---|---|---|---|---|
| 37 | 28 | $1.0 \times 10^{-7}$ | 0.100 | $2.80 \times 10^{9}$ |
| 30 | 31 | $1.0 \times 10^{-7}$ | 0.100 | $3.10 \times 10^{9}$ |
| 30 | 253 | $1.0 \times 10^{-6}$ | 0.100 | $2.53 \times 10^{9}$ |
| 25 | 35 | $1.0 \times 10^{-7}$ | 0.100 | $3.50 \times 10^{9}$ |
| **PFU's/mL ± σ** | | | | **(2.98 ± 0.42) x $10^{9}$** |

was carried out in triplicate, with each plate being incubated during 24 h at a different temperature, viz. 30 °C, 37 °C and 25 °C, so as to verify the optimum temperature for the bacterial phage infection. Following incubation, the plates were visually inspected for the presence of plaques and the number of plaque-forming units (PFU's) was duly counted in each bacterial lawn, after which the following equation was applied (Table 1):

$$\text{Phage particle concentration(PFU/mL)} = \text{Number of PFU's} \times \frac{1}{\text{Dilution}} \times \frac{1}{V_{\text{inoculum}}(\text{mL})}$$

### 2.2.2. Preparation of a W/O/W ME housing bacteriophage particles

The process for producing the W/O/W multiple emulsions (ME) housing phage particles was carried out pursuing the methodology described in detail by Glasser et al. [8,31]. The general compositions of the W/O/W ME formulations produced are displayed in Table 2.

### 2.2.3. Determination of the encapsulation efficiency

For determination of the encapsulation efficiency, a spectrophotometric assay was developed to quantify the phage particles in suspension before and after the process of ME production. Departing from the phage titer calculated from microbiological procedures, five dilutions in ultrapure water (up to a total volume of 5.0 mL) using different volumes of the concentrated phage suspension (PS) produced were prepared, and absorbance of the resulting dilutions was determined at both 255 nm (producing the maximum absorption of the concentrated PS) and 320 nm (where there is little light absorption from phage chromophores) (Table 3). Subtracting $A_{320}$ is meant to correct crudely for light scattering from phage particles and non-phage particulate contaminants.

Performing a linear fitting to the data displayed in Table 3, the equation $Abs_{255nm}$-$Abs_{320nm}$ = $8.3487 \times 10^{-9}$-0.5696 ($r^2$ = 0.99887) was obtained, and applying the equation of Beer-Lambert to the data allowed one to obtain the molar extinction coefficient of phage JG004 (whole) particles as $\varepsilon = 8.3487 \times 10^{-09}$ (PFU's/mL)$^{-1}$ Cm$^{-1}$, and writing a formula for calculating the physical phage particle concentrations:

Phage particle concentration = $\frac{Abs_{@255nm}\text{-}Abs_{@320nm}}{8.3487 \times 10^{-9}}$ virions·mL$^{-1}$. This equation was then applied to calculate the concentration of phage particles (virions/mL) in the ME supernatant following centrifugation at 12500 rpm during 10 min at 4 °C. For these determinations, 2 mL-aliquots of ME were poured into Eppendorf tubes and centrifuged at 12500 rpm during 10 min at 4 °C. Following centrifugation, 200 µL of the supernatant were carefully collected, diluted to 2000 µL with ultrapure water, poured into a quartz cuvette and the absorbance read at 255 nm and 320 nm. For auto-zeroing the spectrophotometer at both wavelengths, a placebo ME was utilized. The efficiency of encapsulation (EE, %) was then determined as $EE(\%) = \frac{i\text{-}s}{i} \times 100$, where ***i*** is the number of phage virions offered initially to prepare the ME and contained in 2-mL of the ME, and ***s*** is the number of phage virions in the supernatant of the 2-mL aliquot following centrifugation.

### 2.2.4. Determination of HS, PI and ZP

For (triplicate) determination of HS, PI and ZP of the aqueous-core lipid nanodroplets by dynamic laser light scattering (DLS), the procedure described by Glasser et al. [8] was pursued, using 1:400 dilutions of ME samples in ultrapure water.

### 2.2.5. Fourier transform InfraRed spectrophotometry (FTIR) analyses

Infrared spectra were produced in the wavenumber range from 4000 cm$^{-1}$ to 400 cm$^{-1}$, with a resolution of 4 cm$^{-1}$ and using Happ-Genzel apodization.

### 2.2.6. X-ray diffraction (XRD) analyses

X-ray diffractograms were produced using X-ray radiation filtered through a Cu target. The X-ray scanning was performed at diffraction angles of 2-Theta (from 5° to 90°, with increments of 0.02 ° and rate of 2°.min$^{-1}$), with a voltage of 40 kV, electric current of 30 mA, and X-ray power of 3 kW.

### 2.2.7. Nanoparticle tracking analysis (NTA)

The system comprised a green-light laser beam at 532 nm and a sCMOS high-resolution camera, to perform the NTA at 25 °C. ME samples were diluted 5000 x (1 µL sample in 4999 µL ultrapure water)

**Table 2**
Composition of the W/O/W multiple emulsions (ME) housing bacteriophage particles (%, w/w).

| Components | | Function in the formulation | % (w/w) | | |
|---|---|---|---|---|---|
| | | | ME10 | ME1000 | MEPLC |
| Internal aqueous phase ($W_{in}$) | Concentrated bacteriophage suspension | Active antibacterial agent | 0.02 (10 µL of concentrated phage suspension) | 2.00 (1000 µL of concentrated phage suspension) | 2.00 (1000 µL of a mixture of LB-top agar (4 mL) and phage-buffer (3 mL)) |
| | | | $1.575 \times 10^{7}$ virions | $1.575 \times 10^{9}$ virions | 0 virions |
| | Tween 80 | Non-ionic | 0.02 | 0.02 | 0.02 |
| | HCl 20 mM | Electrolyte | 1.96 | – | – |
| | HCl 1000 mM | | – | 0.04 | 0.04 |
| Oily phase (O) | Softisan100™ | Lipid | 1.00 | 1.00 | 1.00 |
| | Soybean phosphatidylcholine | Lipophilic surfactant | 0.75 | 0.75 | 0.75 |
| | Glycerol | Protector, co-surfactant | 12.60 | 12.60 | 12.60 |
| External aqueous phase ($W_{ext}$) | Poloxamer P188 | Hydrophilic surfactant | 0.50 | 0.50 | 0.50 |
| | Methylparaben | Preservative, antifungal | 0.10 | 0.10 | 0.10 |
| | Ultrapure water | Diluent | 83.05 | 82.99 | 82.99 |
| TOTAL | | | 100.00 | 100.00 | 100.00 |

**Table 3**
Data utilized to prepare a calibration curve aiming at determining the molar extinction coefficient of bacteriophage JG004 (whole) particles.

| Sample volume of concentrated bacteriophage suspension (μL) | Final volume of dilution (mL) | Number of PFU's in the sample volume of concentrated bacteriophage suspension | Phage particle concentration (PFUs/mL) | $Abs_{255nm}$ | $Abs_{320nm}$ | $Abs_{255nm}$-$Abs_{320nm}$ |
|---|---|---|---|---|---|---|
| 150.00 | 5.00 | $4.47 \times 10^8$ | $8.95 \times 10^7$ | 0.2450 | 0.0510 | 0.1940 |
| 200.00 | 5.00 | $5.97 \times 10^8$ | $1.19 \times 10^8$ | 0.5230 | 0.1080 | 0.4150 |
| 250.00 | 5.00 | $7.46 \times 10^8$ | $1.49 \times 10^8$ | 0.8840 | 0.1830 | 0.7010 |
| 300.00 | 5.00 | $8.95 \times 10^8$ | $1.79 \times 10^8$ | 1.1800 | 0.2430 | 0.9370 |
| 350.00 | 5.00 | $1.04 \times 10^9$ | $2.09 \times 10^8$ | 1.5040 | 0.3140 | 1.1900 |

before performing the NTA analyses.

*2.2.8. Thermal analyses via thermogravimetry (TGA) and differential scanning calorimetry (DSC)*

Thermal characterization followed the procedure described by Glasser et al. [8], using 19–34 mg for the TGA analyses and 21–26 mg for the DSC analyses.

*2.2.9. Antimicrobial (lytic) activity of the W/O/W multiple emulsions housing bacteriophage particles*

MEs housing phage particles were subjected to testing for lysis halos following application of samples of ME on a bacterial lawn of *P. aeruginosa*. For extration of the phage particles, 500 μL chloroform were added to 1000 μL ME housing phage particles in a test tube. The resulting suspension was gently shaken in a vortex during 5 s and centrifuged at 5500 rpm (10 min, 4 °C). Following centrifugation, the supernatant was immediately recovered and subjected to antimicrobial testing. This procedure was also repeated for the MEPLC. Into a test tube containing 3 mL LB-top agar, 100 μL bacterial suspension (*P. aeruginosa* grown at 37 °C during 18 h in LB broth) were added. After mild stirring, this suspension was poured into a Petri plate previously prepared with LB-bottom agar, and allowed to solidify at room temperature. Each Petri plate was divided into four quadrants and the samples were added according to two methods: **(i)** disk test, where a sterile filter disk was placed in the centre of each quadrant and on top of each disk one applied, separately, 20 μL of supernatant sample containing phages recovered previously from the ME housing phage particles, 20 μL of supernatant sample obtained from the placebo ME, 10 μL of the concentrated stock-PS (positive control) and 10 μL of the placebo of the stock PS (negative control); **(ii)** droplet test, where a small droplet was applied in the centre of each quadrant, directly on top of the solid LB-bottom agar, separately, 20 μL of supernatant sample containing phages recovered previously from the ME housing phage particles, 20 μL of supernatant sample obtained from the placebo ME, 10 μL of the concentrated stock-PS (positive control) and 10 μL of the placebo of the stock PS (negative control). The Petri plates were incubated at 37 °C during 24 h, after which they were visually inspected for the presence of lysis halos. To test wether chloroform exerted any deleterious action upon the phage particles, during the extraction process from the ME, another test was also performed exclusively for the (a) ME1000, and (b) MEPLC systems, with and without phage particle extraction using chloroform, using the aforementioned disk test approach.

*2.2.10. (Cryo-/NS-) transmission electron microscopy analyses*

Carbon grids were prepared using undiluted as well as diluted (1:5, in ultrapure water) samples of ME1000, MEPLC and concentrated PS. For the **Negative Staining (NS),** samples were prepared exactly in the same way as described by Glasser et al. [8]. For **cryo-freezing in amorphous ice**, the samples were prepared in Lacey Carbon Type A 300 mesh copper grids (Ted Pella Inc., Redding CA, U.S.A.), which were previously submitted to a Glow Discharge process in an easiGlow device (PELCO, Redding CA, U.S.A.) (electric current of 15 mA, negative charge, 25 s discharge). Freezing in amorphous ice (cryo-preparation) was carried out using a *Vitrobot Mark IV* equipment (FEI, Eindhoven, The Netherlands) with controlled temperature (22 °C) and relative humidity (100%). For preparing the cryo-samples, 3 μL of the samples were dropped on the grids and allowed to settle for 20 s. The grids were then blotted for 3 s and vitrified by rapidly plunging into liquid ethane at −145 °C, after which the grids were kept in liquid nitrogen at −196 °C until the moment of analysis in the microscope, and maintained at −173 °C in the chamber of the microscope during the whole analysis timeframe. Pure ME1000 samples were also prepared simply by pouring tiny (3 μL) droplets directly on top of carbon grids (not subjected to the *Glow Discharge* procedure), without any type of treatment or staining, followed by removal of the excess sample using filter paper, allowing to dry first at room temperature during 1 h, and subsequently in a vacuum chamber at room temperature during 7 days, prior to carrying out TEM analyses. The **electron microscope analyses** were then carried out as described by Glasser et al. [8].

*2.2.11. Determination of the cytotoxicity potential of the W/O/W ME systems, via the MTT assay*

For cell proliferation, DMEM supplemented with bovine fetal serum (10%, w/w) and antibiotic (100 $UI_{penicillin}$/mL plus 100 $\mu L_{streptomycin\ sulfate}$) (1%, w/w) was used, at pH 7.4 and 37 °C, under a humid atmosphere containing 5% $CO_2$. Upon reaching confluence, the cells (V79 and A549) were disadhered by using trypsin. Plating out was performed by inoculating ca. $1 \times 10^4$ viable cells in each well of a 96-well microplate, using 100 μL sample, followed by incubation for 48 h until semi-confluence was reached. Cell viability analysis using MTT began with plating of a cell suspension containing $0.5 \times 10^5$ cells/mL. After 24 h (time needed for cell adherence and stability) the cells were placed in contact with the samples (ME10, ME1000, MEPLC, and PS and its placebo) for an extra 24 h, in volume concentrations from 0 to 17.5% (v/v). The plates were then kept for 24 h in a heating cabinet set at 37 °C with 5% $CO_2$. After this step, the samples were washed away with sterile PBS buffer and the cells exposed to MTT (0.5 mg/mL). Cellular viability was determined using reduction of MTT. After 3 h at 37 °C and 5% $CO_2$, the number of viable cells was determined by measuring the amount of MTT converted to formazan (a purple compound) by the mitochondrial dehydrogenases. For this, 100 μL DMSO were added to each well and absorbance readings performed at 570 nm in an ELISA microplate reader. All tests were performed in quintuplicate for each concentration of sample tested. The analysis of results was carried out assuming as 100% of cell viability the average of the absorbance values obtained for the untreated control.

*2.2.12. Determination of the apoptosis and necrosis potential of the W/O/W ME systems, via image cytometry (Tali® analysis)*

The cells that had been treated with diluted samples (concentrated PS, MEPLC, ME10 and ME1000) at a concentration of 10% of that of the departing samples, during 24 h, were centrifuged and concentrated to $1 \times 10^6$ cells/mL. 100 μL-aliquots of this cell suspension were prepared according to the specifications of the Tali® Apoptosis Kit, and tests performed in triplicate. After treatment, the content was transferred to 2 mL-test tubes, centrifuged at 1500 rpm for 5 min, and the resulting supernatant discarded. The remaining material was resuspended with 100 μL *Annexin binding buffer (ABB)*, 5 μL *Annexin V Alexa Fluor® 488* were added, and the contents maintained in the dark at room temperature during 20 min. After this period, the material was centrifuged

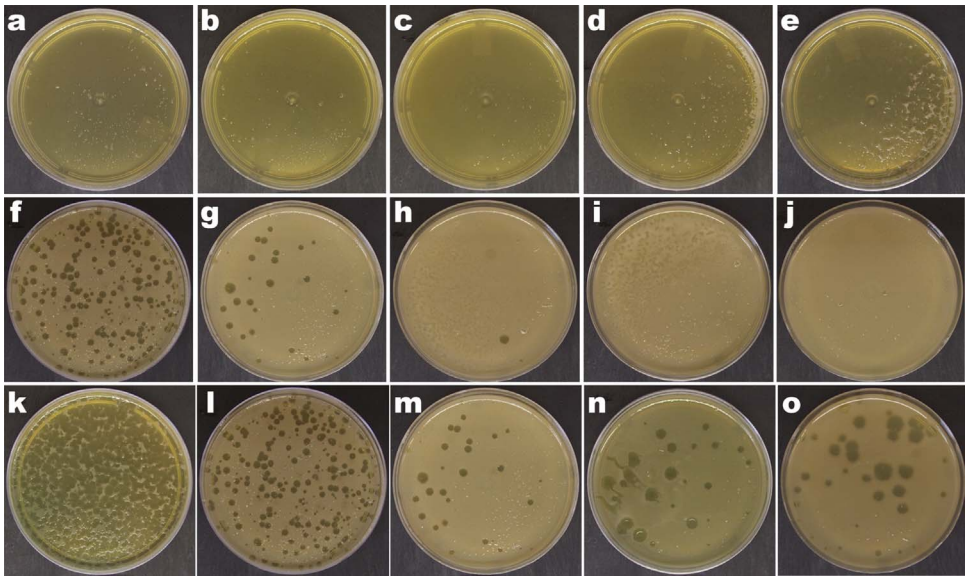


**Fig. 1.** Results from phage JG004 propagation trials in its *Pseudomonas aeruginosa* host, showing the formation of plaque forming units (PFUs) for the whole range of serial dilutions of the stock-solution of bacteriophage JG004: **(a)** $10^{-1}$, **(b)** $10^{-2}$, **(c)** $10^{-3}$, **(d)** $10^{-4}$, **(e)** $10^{-5}$, **(f)** $10^{-6}$, **(g)** $10^{-7}$, **(h)** $10^{-8}$, **(i)** $10^{-9}$, **(j)** $10^{-10}$; The microbiological quantification of the titer of bacteriophage concentrated suspension is displayed in figures k-o: **(k)** $10^{-5}$, 30 °C, > 300 PFUs; **(l)** $10^{-6}$, 30 °C, 253 PFUs; **(m)** $10^{-7}$, 30 °C, 31 PFUs; **(n)** $10^{-7}$, 37 °C, 28 PFUs; **(o)** $10^{-7}$, 25 °C, 35 PFUs.

at 1500 rpm for 5 min, the supernatant was removed and 100 µL of *Annexin binding buffer (ABB)* and 1 µL of Tali™ *Propidium Iodide* (PI) were added, with the resulting solution being left standing for 5 min at room temperature. The resulting material (25 µL) was placed in a specific glass slide for reading, and viability, apoptosis and necrosis were evaluated. Relative indexes of necrosis and apoptosis of the treated groups (samples) were measured by considering the ratio of the values of necrosis and apoptosis of the treated groups relative to the negative control group.

#### 2.2.13. Formulation of isotonic solutions (IS) integrating the W/O/W ME1000 system, aiming at administration via nebulization, and assessment of their antibacterial activity

Either 30 µL, 60 µL or 90 µL of ME1000 were added to 10 mL sterile saline solution at 0.9% (w/v) NaCl in ultrapure water in separate (sterilized) Falcon flasks and duly homogenized via gentle shaking. For determination of the antibacterial potential of these ISs, either 500 µL or 1000 µL were poured into a test tube containing 4 mL top agar and 300 µL bacterial suspension (*P. aeruginosa* grown at 37 °C during 18 h in LB broth). After mild stirring, the top agar containing the bacterial suspension and the added IS was poured into a Petri plate, previously prepared with 25 mL LB-bottom agar, and allowed to solidify at room temperature. The Petri plates were then incubated at 37 °C during 24 h and, following the incubation period, they were visually inspected for the presence of lysis halos.

#### 2.2.14. Determination of the DNA damage potential of the IS integrating the W/O/W ME1000 system, via the comet™ assay

Each treatment group involved 10 µL of cells (V79-4, A549, and 3T3 fibroblasts) in 110 µL of low melting point agarose (0.6%, w/v), with the mixtures being placed onto microscope slides that had been pre-coated with normal melting point agarose (1.5%, w/v). Coverslips were positioned over the samples in the microscope slides, and the slides were placed at 4 °C for polymerization to occur. Following polymerization, coverslips were removed and the slides treated with an ice-cold (4 °C) lysis solution during 60 min. The treatment groups were then incubated in an electrophoresis buffer (pH 13) during 20 min, followed by electrophoretic analysis for 20 min at 1.3 V/cm. After electrophoresis, the slides were covered with a neutralizing solution for 5 min, washed three times with distilled water, and allowed to stand overnight at room temperature. Prior to staining, the dry slides were left in a fixing solution for 10 min, after which they were further washed three times with ultrapure water. Following these procedures, the slides were allowed to stand at room temperature for 1.5 h, after which they were rehydrated with ultrapure water and stained for approximately 15 min with a silver staining solution. Subsequently, the slides were bathed in ultrapure water and then in a stop solution (acetic acid, 1% (v/v)). Finally, the slides were again gently washed with ultrapure water and allowed to dry at room temperature. Silver staining is analogous to fluorescence, during which the positive charge of the silver cations enables them to bind to DNA and DNA fragments, producing the characteristic color. Analyses were performed using a Zeiss Axiovert-60 optical microscope, and at least 100 cells were counted on each slide, with 3 slides for each test (ca. 300 cells). The analyses were carried out in triplicate, totaling 900 cells for the analysis of each IS tested. The Comet assay analyses were performed by assigning a score from 0 to 4 [42]. For this visual method, the number of cells found for each score was multiplied by the value of the score; all the values were summed at the end of the analysis of each slide. Because the score depended on the number of cells observed, an index of tail damage (or DNA damage) was created by normalizing the score given to the slide by the number of cells analyzed on the slide.

## 3. Results and discussion

### 3.1. Propagation, purification and quantification of bacteriophage JG004

Propagation of the phage particles in the stock-suspension in its specific host (*P. aeruginosa*) (Fig. 1a–j) resulted in a concentrated PS, and was followed by determination of the phage titer.

Plating serial decimal dilutions of this concentrated PS, as described in Section 2.2.1, allowed determination of the number of plaque-forming units (PFUs) (Fig. 1k–o) for selected serial dilutions. It is possible to observe the formation of a phage lawn for the smaller dilutions, up to $1 \times 10^{-5}$, indicating a complete propagation of the phage and concomitant lysis of all bacterial cells (Fig. 1a–j). Each plaque of lysis corresponds to one unit of phage. Incubation of the bacteria with the phage at three different temperatures (30 °C, 37 °C and 25 °C) did not show any difference in phage proliferation (Figs. 1k-o), thus providing indication that both phage and bacteria demonstrate a similar activity within this range of temperatures (Fig. 1k–o). An average phage particle concentration of $(2.983 \pm 0.416)x10^9$ virions/mL (Fig. 1k–o) was thus obtained for the concentrated PS following propagation of the stock-suspension. A minimum absorption could be observed around 245 nm; when this minimum is absent from the spectrum, many contaminants are likely present in the suspension which often happens

when its contains fewer virions. This was not the case, however, with the concentrated PS produced. Performing a linear fitting to the data displayed in Table 3, and applying the equation of Beer-Lambert to the data allowed calculation of the molar extinction coefficient of phage JG004 (whole) particles as $\varepsilon = 8.3487 \times 10^{-09}$ (PFU's/mL)$^{-1}$ Cm$^{-1}$. The physical phage particle concentration in the concentrated PS was then calculated as $1.575 \times 10^{9}$ virions/mL, as described in Section 2.2.3. The concentration of phage particles obtained from spectrophotometric readings was thus of the same order of magnitude but ca. 47% lower than that obtained from microbiological procedures. Taking into consideration the large amount of physical phage particles in the concentrated suspension, the results obtained from spectrophotometric readings are suitable, e.g. for the quantification of the encapsulation efficiency, since a ratio of values calculated from this procedure will virtually eliminate any error of the determination.

### 3.2. HS, PI and ZP

A previous work on the statistical optimization of the formulation parameters leading to production of a stable W/O/W ME [31], following an experimental full factorial design, has set as mandatory variables high levels of protein entity and lipophilic surfactant (viz. lecithin) and a low level of hydrophilic surfactant (viz. poloxamer P188), and a high-homogenization stirring speed. Following this set of (optimized) processing parameters, three W/O/W ME were produced (Table 2), viz. ME10, ME1000, and MEPLC. The results obtained from the analysis by DLS of the several W/O/W ME are displayed in Fig. 2.

A larger amount of physical phage particles did not lead to any changes in ZP values (Fig. 2c), but enhanced the antibacterial properties of the ME (as will be discussed in Section 3.8). The easiest way to stabilize the system is to reduce surface tension, so as to decrease the free energy derived from the expansion of the overall surface area [43]. Thus, we opted to increase the lipophilic surfactant level in producing the ME, since tensioactive agents do play an important role in stabilizing emulsions. However, most surfactants cannot reduce the interfacial tension to levels enough to counteract all the surface free energy caused by the tremendous increase in surface area during homogenization, and thus emulsions are usually considered thermodynamically unstable systems [40,44,45]. As can be seen in Fig. 2, production of ME10 and ME1000 systems led to quite homogeneous particles. Storage of these ME systems with encapsulated phage particles (Fig. 2) throughout nearly one year at 4 °C led to maintenance of the particle HS between 159 and 165 nm (ME10) and between 176 and 189 nm (ME1000) (Fig. 2a), to a small increase of the PI during the first seven days (Fig. 2b), and to a small increase in the values of ZP during the first seven days presumably due to ion concentration at lipid nanodroplets interface (Fig. 2c). A placebo ME was also produced, without encapsulated phage particles, and stored for nearly one year under the same conditions; for this, the very same trend was found for the average particle HS, together with a slight increase in ZP values. Increasing molecular weight (as in Softisan 100™, with $C_{10}$–$C_{18}$ fatty acid moieties) and decreasing dielectric constant (as in Tween 80) indicates a greater hydrophobicity, leading to a greater impregnation of the interface and to a more stable ME [8,32,46], which is in clear agreement with the stability observed for our ME systems, both in terms of maintenance of average particle HS and PI, and ZP values. The superior stability of emulsions containing Tween 80 can be linked to the fact that Tween 80 possesses an oleate-chain and one unsaturated bond, which leads to a more stable O/W interface layer and subsequently to higher emulsion stability [40]. The higher hydrophobicity of our ME systems is further supported by the (calculated) weighted HLB average value (13.418). To produce this value of HLB, the weighted HLB expression by Schmidts et al. [40] was duly applied [8].

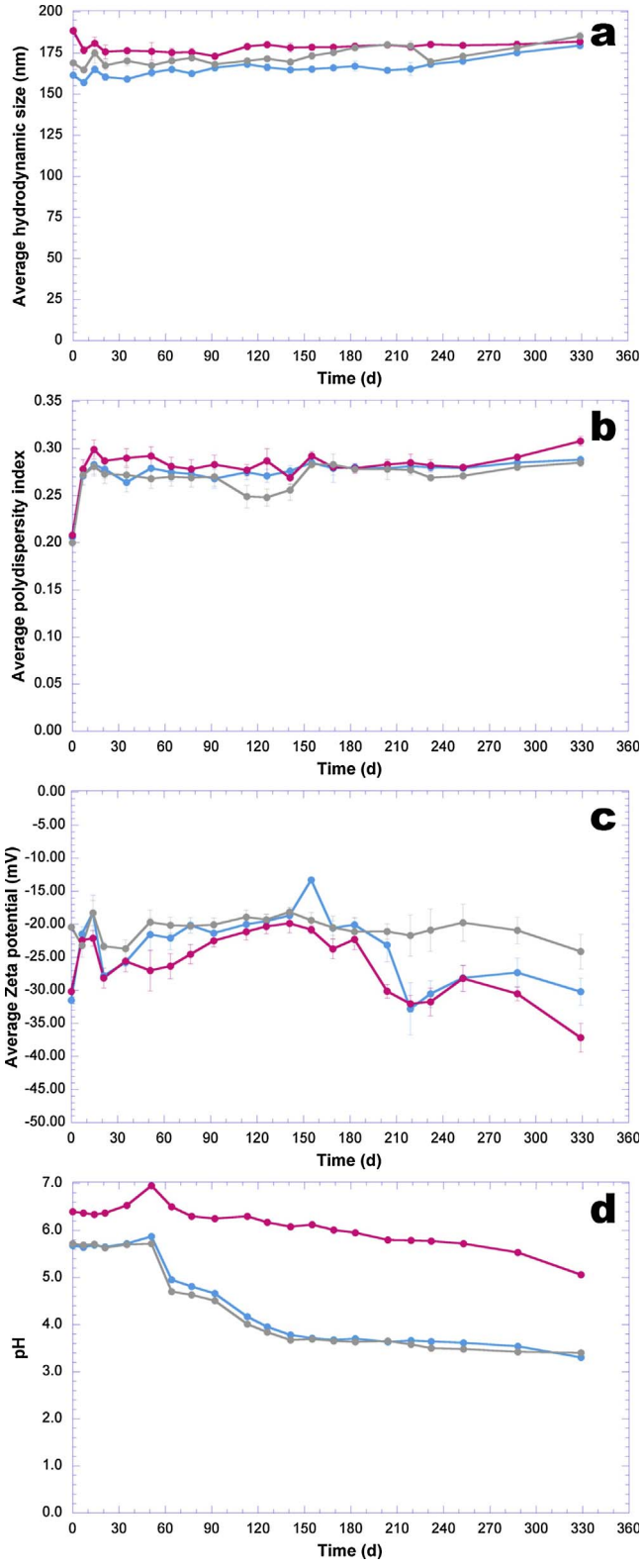


**Fig. 2.** Time evolution of average (n = 3) and associated σ of **(a)** HS, **(b)** PI, **(c)** ZP and **(d)** pH of lipid nanodroplets encasing phage particle moieties, integrating the ME systems, throughout storage time (light blue circles, ME10; pink circles, ME1000; gray circles, MEPLC). (For interpretation of the references to colour in this figure legend, the reader is referred to the web version of this article.)

### 3.3. Encapsulation efficiency

Following centrifugation of 2-mL aliquots of both ME1000 and MEPLC, 200 µL of ME1000 supernatant were carefully collected, diluted to 2000 µL with ultrapure water and the absorbance read at 255 nm and 320 nm using quartz cuvettes, using MEPLC as blank at both wavelengths. Using this same approach for the concentrated PS, with 40 µL supernatant diluted to 2000 µL with ultrapure water (i.e. 1:50 dilution), where a blank was prepared using a mixture of LB-top agar (4 mL) and phage-buffer (3 mL) to auto-zeroing the spectrophotometer at both wavelengths producing $Abs_{255nm}$-$Abs_{320nm}$ = 0.263, a concentration of phage particles in the concentrated PS was calculated as $1.575 \times 10^9$ virions/mL, as described in Section 2.2.3. Using the results obtained from absorbance readings ($Abs_{255nm}$-$Abs_{320nm}$ = 0.142) with the supernatant of ME1000, a phage particle concentration of $1.701 \times 10^8$ virions/mL was obtained for ME1000 supernatant. Using the equation displayed in Section 2.2.3, where the amount of virions offered to prepare 2 mL of ME1000 was equal to $3.150 \times 10^9$ virions and the amount of virions in the supernatant of 2 mL of ME1000 was equal to $3.402 \times 10^8$ virions, the phage particle encapsulation efficiency (EE) of ME1000 was EE = 89.2%. This EE is related solely to phage virions, since absorbance readings were made so as to exclude cell debris and any other intracytoplasmatic proteins released upon bacterial cell lysis.

### 3.4. FTIR analyses

Fig. 3 displays the infrared spectra of MEPLC (Fig. 3d), ME10 (Fig. 3e), ME1000 (Fig. 3f), and concentrated PS (Fig. 3g).

The intensity peaks at wavenumbers 3300 $cm^{-1}$ (MEPLC, Fig. 3d), 3300 $cm^{-1}$ (ME10, Fig. 3e), 3350 $cm^{-1}$ (ME1000, Fig. 3f) and 3250 $cm^{-1}$ (concentrated PS, Fig. 3g) are characteristic of −OH group stretching and indicate the presence of bonding with water molecules. These peaks are more intense in Fig. 3d–f due to the aqueous nature of the ME produced. In Fig. 3d–f one can observe peaks between 2853 and 2924 $cm^{-1}$ (characteristic of $sp^3$ CH stretches), 1746 $cm^{-1}$ (Fig. 3d) and 1742 $cm^{-1}$ (Fig. 3e and f), characteristic of C═O stretch (dimer, H-bonded), and in Fig. 3g a peak at 1600 $cm^{-1}$, characteristic of −C═O. In the infrared spectrum of the concentrated PS (Fig. 3g), a peak that appears at 2931 $cm^{-1}$ is probably attributable to $CH_2$ asymmetrical stretch, a peak that appears at 1525 $cm^{-1}$ is probably attributable to the angular deformation of a $-NH_2$ group (either the terminal amine group or an amine group of lysin moieties in the capsular or tail fiber protein entities), a peak appearing at 1399 $cm^{-1}$ is probably attributable to a C−O−H in-plane bend, another peak appearing at 1457 $cm^{-1}$ is most likely attributable to the −COO-, a peak appearing at 1067 $cm^{-1}$ probably attributable to $PO_4$, a peak appearing at 985 $cm^{-1}$ is probably attributable to an out-of-plane O−H bend, and a peak appearing at 1243 $cm^{-1}$ probably attributable to C−O stretch. Comparing the infrared spectra of ME without (Fig. 3d) and with (Fig. 3e and f) encapsulated phage particles, peaks are visible in the region from 1107 to 1030 $cm^{-1}$, characteristics of −C═O bends. In the infrared spectra of concentrated PS (Fig. 3g), a characteristic peak appears at 1067 $cm^{-1}$ due to the stretching of the −P−O− bond in phosphate groups. A comparison between the infrared spectra of ME without (Fig. 3d) and with (Fig. 3e and f) encapsulated phage particles, may lead to the conclusion that there are no displacement of major peaks, neither the existence of the characteristic peaks of the infrared spectrum of free phage particles (1525 $cm^{-1}$, 1399 $cm^{-1}$, 620 $cm^{-1}$ and 533 $cm^{-1}$ (this last one probably attributable to C−C bends)), which indicates that nearly all phage particles offered in the preparation of ME10 and ME1000 were in fact encapsulated, being therefore virtually absent in the external aqueous phase of the ME. Additionally, comparing the infrared spectra of ME with encapsulated phage particles (Fig. 3e and 3f), a characteristic peak at 1107 $cm^{-1}$ (Fig. 3e) and 1101 $cm^{-1}$ (Fig. 3f) with a higher intensity in Fig. 3f, further indicates the presence of higher amounts of phage particles in the later.

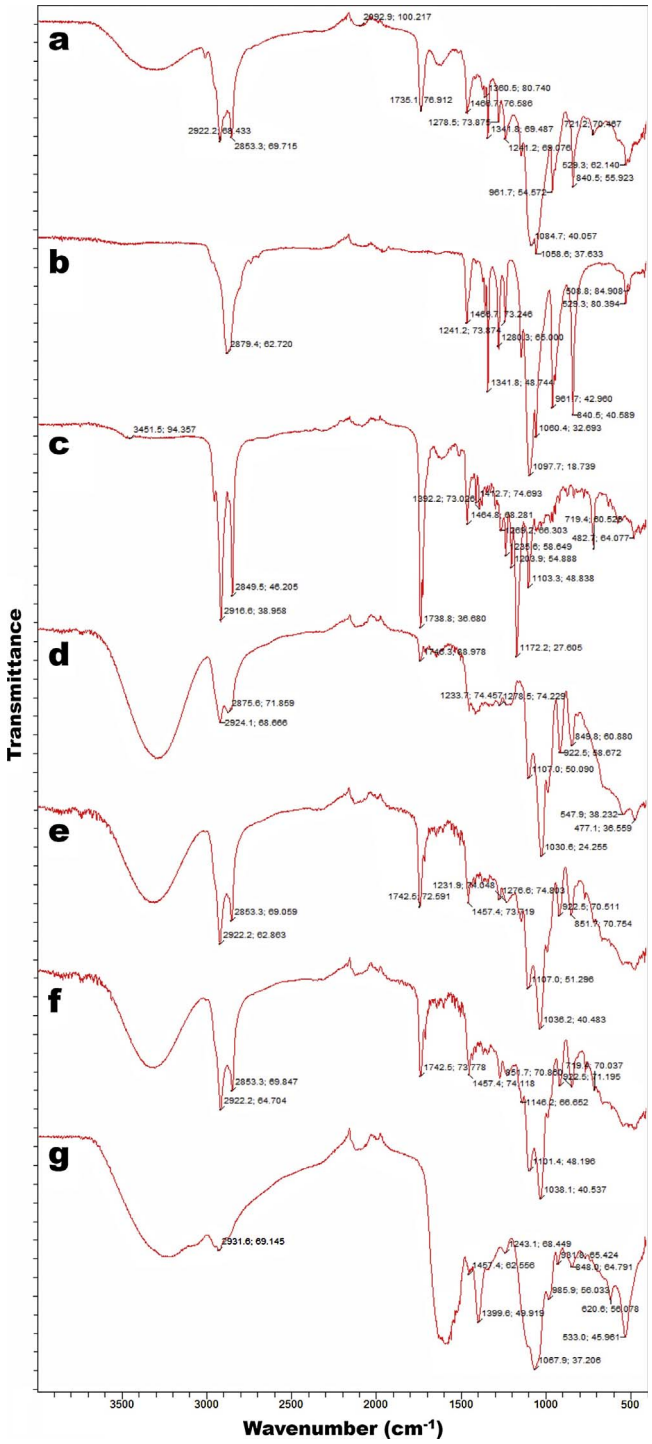


**Fig. 3.** FTIR spectra of samples of **(a)** lecithin, **(b)** poloxamer 188, **(c)** Softisan100™, **(d)** MEPLC, **(e)** ME10, **(f)** ME1000, and **(g)** concentrated bacteriophage suspension.

### 3.5. XRD analyses

The results obtained from the X-ray diffraction analyses performed to the concentrated PS and to MEPLC and ME1000 are displayed in Fig. 4 as normalized diffractograms.

Since the intensity of peaks in the X-ray diffraction patterns also depends on the concentration of bioactive entity, an increase in both the intensity of peaks and diffraction pattern was expected for ME10 and ME1000 (Fig. 4 and zoomed insertion) relative to MEPLC (zoomed

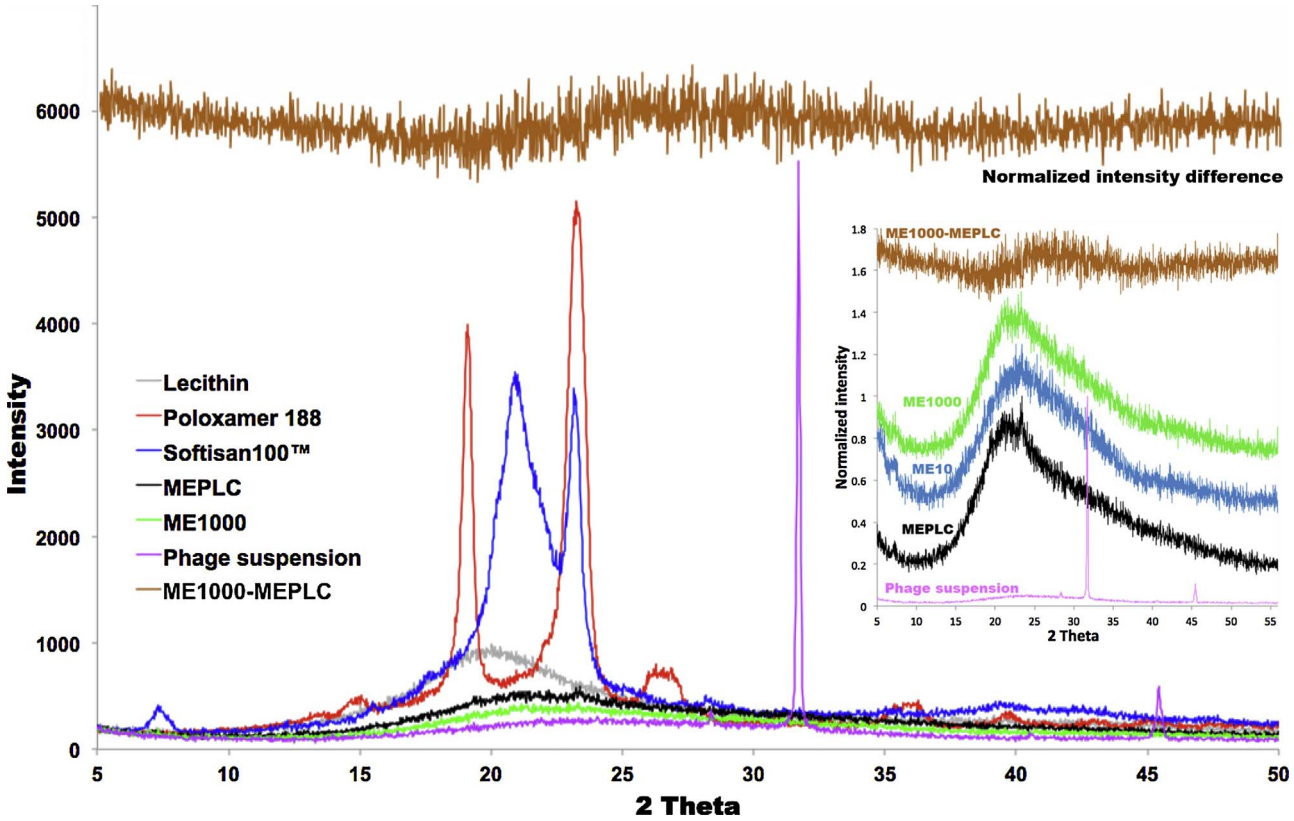


**Fig. 4.** X-ray diffractograms (XRD) of samples of lecithin (grey), poloxamer 188 (red), Softisan100™ (blue), MEPLC (black), ME1000 (green), and of the concentrated bacteriophage suspension (purple). The diffractogram in the brown curve was produced by subtracting the normalized MEPLC diffractogram from that of ME1000. (For interpretation of the references to colour in this figure legend, the reader is referred to the web version of this article.)

insertion in Fig. 4). The diffractograms of MEPLC, ME10 and ME1000 exhibited a wide noisy band, with defined peaks in the region of $18.00 \leq 2\text{Theta} \leq 25.00$, where the smaller and well-defined peaks produced indicate crystalline residues of the lipid (Softisan 100™) utilized in the preparation of the ME. In particular, the X-ray diffractograms revealed the presence of two signals, one at $2\theta = 21.50^{\circ}$ and another at $2\theta = 23.26^{\circ}$ (MEPLC, ME10 and ME1000, zoomed insertion in Fig. 4), which are both characteristic of the orthorhombic polymorphic form frequently observed in complex triacylglycerols such as Softisan 100™ [47]. Subtraction of MEPLC diffractogram from ME1000 diffractogram (i.e. ME1000-MEPLC) allowed cancellation of the effect of the lipid matrix integrating the aqueous-core nanodroplets and clearly does not show peaks that stand out on the curve. This allows to conclude that the amount of phage particles in the external aqueous phase was too small to absorb energy from the X-rays hitting the sample, and thus observe the amorphous character of the lipid nanodroplets housing phage particles. This conclusion is in fact supported by the shallow peak observed in curve ME1000-MEPLC in the region of $19.00 \leq 2\text{Theta} \leq 40.00$ (Fig. 4).

### 3.6. NTA analyses

The samples (1 μL sample previously diluted in 4999 μL ultrapure water) were hit by a green-light laser beam at 532 nm and the Brownian motions of the lipid nanodroplets were captured by a sCMOS high-resolution camera, to perform NTA, allowing to observe the absence of aggregation phenomena. This analysis (performed in quintuplicate) allowed one to calculate the diffusion coefficient of the lipid nanodroplets integrating ME1000. Particle concentration in the ME was determined as $2.39 \times 10^{12}$ particles/mL, with a dynamic viscosity of $\eta = 0.888704$ cP (or 0.000888704 kg/(m.s)). Assuming a homogeneous hydrodynamic particle diameter for the lipid nanodroplets in ME1000 of 188.54 nm, the diffusion coefficient of the lipid nanodroplets housing phage particles could be calculated using the Stokes-Einstein equation, viz. $D = \frac{k_B \cdot T}{6 \cdot \pi \cdot \eta \cdot r}$, where $D$ is the diffusion coefficient, $k_B$ is the Boltzmann's constant ($1.3806488 \times 10^{-23}$ m$^2$ kg/(s$^2$ K)), $T$ is the absolute temperature (K), $\eta$ is the dynamic viscosity (kg/(m.s)), and $r$ is the hydrodynamic radius (m) of a spherical particle. The diffusion coefficient of the lipid nanodroplets integrating ME1000 was calculated as $2.607 \times 10^{-12}$ m$^2$ s$^{-1}$. Most notably, this result is comparable and of the same order of magnitude ($10^{-12}$ m$^2$ s$^{-1}$) as the results published by Glasser et al. [8] and Katayama et al. [48]. Diffusion coefficients for molecules fall usually in the range $10^{-10}$–$10^{-7}$ m$^2$ s$^{-1}$, but diffusion coefficients for nanoparticles are typically of the order of magnitude of $10^{-12}$ m$^2$ s$^{-1}$ [48]. Lecithin has been reported to stabilize W/O/W ME [40], with the increased stability being related to a change in the diffusion coefficient of water and water-soluble substances subject to the oily-phase composition. ME stability is negatively correlated with the diffusion coefficient, with a higher stability being associated with a lower diffusion coefficient [40,48].

### 3.7. TGA and DSC analyses

A close inspection of the thermogravimetric curves (Fig. 5a) of W/O/W ME systems, allows identification of two major mass loss events, attributable to water loss. The first water loss event occurs from about 50 °C up to 110 °C, probably related to water loss from the external aqueous phase. The second water loss event, extending from ca. 120 °C up to 185 °C, is most likely linked to the loss of the lipid constituent of the nanodroplets with concomitant water loss from the internal aqueous phase. As expected, the thermogravimetric curve of the concentrated PS exhibited only one major mass loss event, entending from about 50 °C up to 105 °C, due to the aqueous nature of the suspension possessing only phage particles and bacterial cell debris. The 1 st

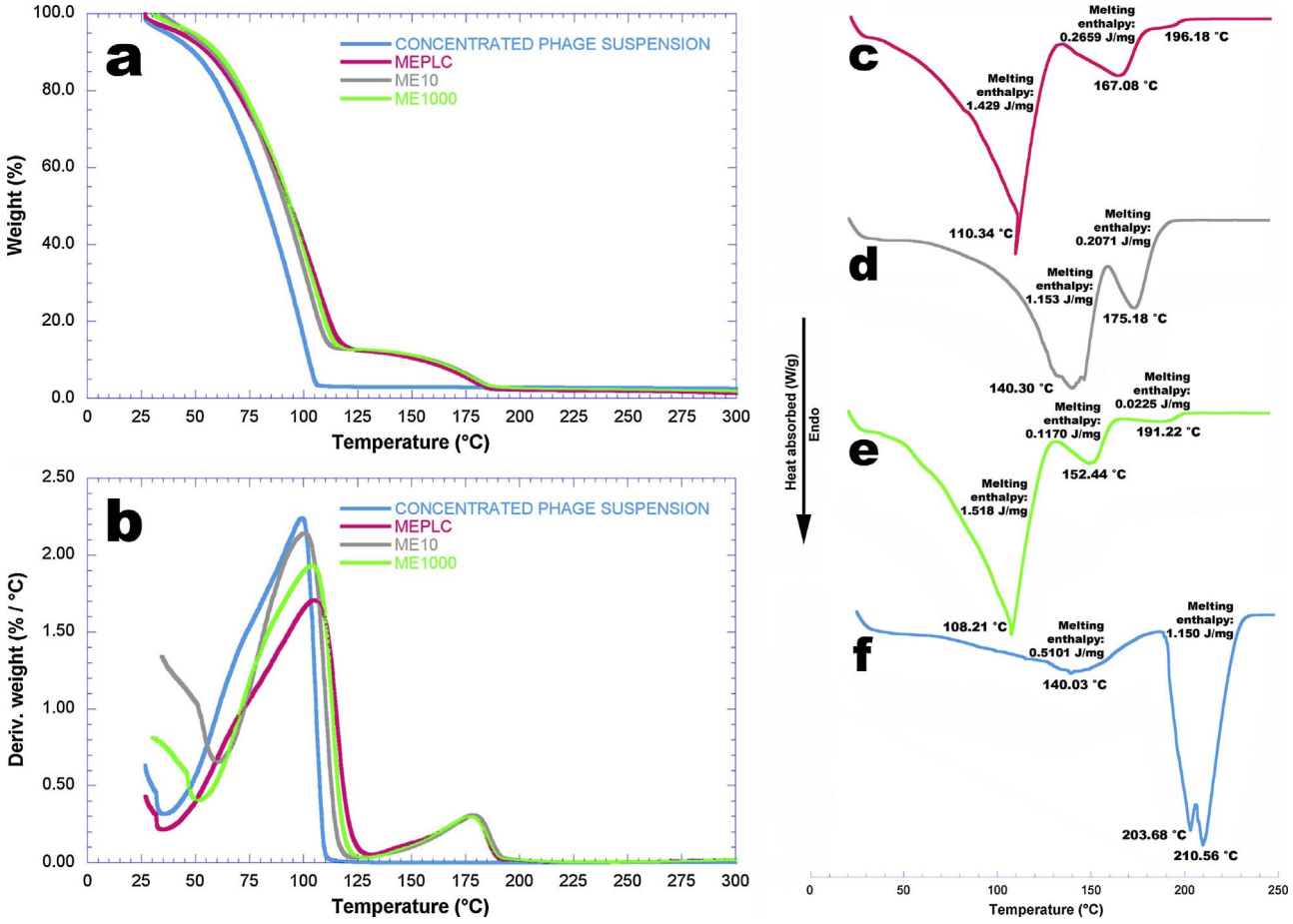


**Fig. 5.** Thermogravimetric curves **(a)** and 1st derivative of the weight loss curves **(b)** of concentrated PS (blue lines), MEPLC (pink lines), ME10 (gray lines), and ME1000 (green lines), and DSC thermograms of **(c)** MEPLC (pink lines), **(d)** ME10 (gray lines), **(e)** ME1000 (green lines), and **(f)** concentrated PS (blue lines). (For interpretation of the references to colour in this figure legend, the reader is referred to the web version of this article.)

derivative of the weight loss curve (i.e., the rate of mass change, Fig. 5b) can be used to tell the points at which weight loss is most apparent (inflection points), viz. 110 °C and 180 °C for MEPLC, 105 °C and 180 °C for ME1000, 100 °C and 180 °C for ME10 and, once more as expected, 100 °C for the concentrated PS. Being essentially inert entities of proteic nature, phage particles are not hygroscopic in nature and thus are not expected to adsorb more water molecules when imprisoned within the aqueous core of the lipid nanodroplets, and in fact this can be observed from a close inspection of Fig. 5a and b, where no displacement in the thermogravimetric curves (Fig. 5a) could be observed for MEPLC, ME10 and ME1000, with water loss from the inner core of the lipid nanodroplets occurring at the same (higher) temperature most probably due to hydrogen bonding between water molecules and Tween 80. This can be confirmed by inspection of Fig. 5b, where such absence of displacement can be seen more clearly in the second peak. ME1000 underwent a two-step weight loss process, and is stable at least up to 50 °C. The TGA analysis of the nanodroplets showed a weight loss of about 87.5% up to 120 °C which can be attributed to the loss of the external water phase from the systems. The lipid nanodroplets matrix system, however, showed a weight loss of about 10% when heated up to 200 °C as shown in Fig. 5a and b.

The results from DSC analyses are displayed in Fig. 5c–f. Imprisonment of phage particles within the aqueous-core lipid nanodroplets promoted a slight decrease in the melting temperature peaks (absorption peaks at 110.34 °C, 167.08 °C and 196.18 °C and associated melting enthalpies of 1.429 J/mg, 0.2659 J/mg and 0 J/mg, respectively, for MEPLC (Fig. 5c), to absorption peaks at ca. 108.21 °C, 152.44 °C and 191.22 °C and associated melting enthalpies of 1.518 J/mg, 0.1170 J/mg and 0.0225 J/mg, respectively, for ME1000 (Fig. 5e)), denoting a shortening of the melting temperature range in the case of ME1000 (Fig. 5c and e). Inclusion of phage particles in the lipid nanodroplets led to a significative decrease in the peak of heat absorption (108.21 °C), when compared with that of the concentrated PS (210.56 °C), due to amorphization of the system. The same trend was noticed when comparing MEPLC and ME1000. When analyzing ME1000, one obtained a melting enthalpy of 1.518 J/$mg_{nanoemulsion}$, at 108.21 °C, a value only 6.23% higher than that of MEPLC, which probably accounts for the stabilizing effect of the nanoencapsulation procedure. These results (Fig. 5c–f) are in close agreement with those obtained from X-ray diffraction (Fig. 4), since as can be seen from inspection of the DSC thermograms, imprisonment of the phage particles within the aqueous core lipid nanodroplets led to a decreased crystallinity with shortening of the melting profile. Amorphization of the lipid envelope upon imprisonment of the phage particles (Figs. 4 and 5 c–f) most likely enhanced the accomodation capability of the lipid nanodroplets for a macromolecule such as a phage particle. Due to decreased rigidity, a reduction in the release rate of entrapped particles was most likely certain, which in turn might explain the high stability observed for the W/O/W ME system with entrapped phage particles (Fig. 2). A close inspection of the DSC thermograms displayed in Fig. 5c–f allows to observe three distinct endothermic events: one at 196.18 °C (MEPLC) that moved to 191.22 °C (ME1000), implying a decrease in crystallinity; one at 167.08 °C (MEPLC) that moved to 152.44 °C (ME1000); and one at 110.34 °C (MEPLC) that moved to 108.21 °C (ME1000). Remarkably, the thermal events depicted in Fig. 5c–f and the X-ray diffractograms depicted in Fig. 4 denote a clear transition from a crystalline state of the

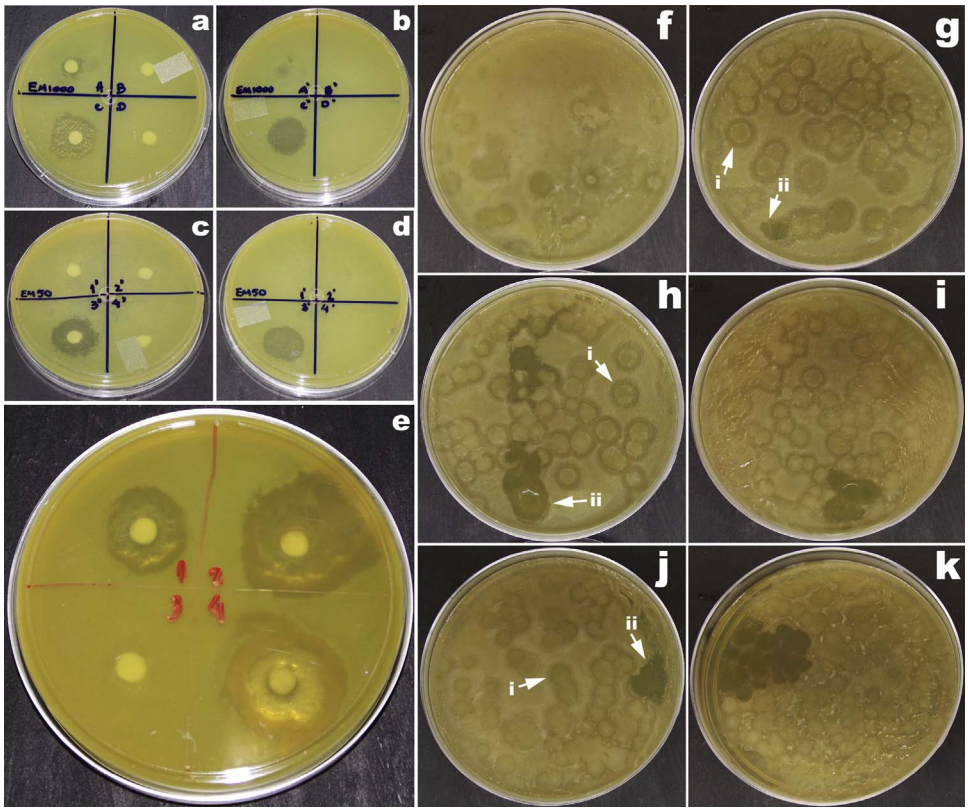


**Fig. 6.** Antimicrobial activity of ME1000 (**a** and **b**) and ME10 (**c** and **d**). Upper left quadrant: 20 μL ME applied on sterile filter paper disk (**a** and **c**) or a 20 μL-droplet of ME (**b** and **d**) applied directly on the surface of LB top agar prepared with 100 μL bacterial suspension of *P. aeruginosa*; Upper right quadrant: 20 μL MEPLC applied on sterile filter paper disk (**a** and **c**) or a 20 μL-droplet of MEPLC (**b** and **d**); Lower left quadrant: 10 μL concentrated bacteriophage suspension applied on sterile filter paper disk (**a** and **c**) or a 10 μL-droplet of concentrated bacteriophage suspension (**b** and **d**); Lower right quadrant: 10 μL sterile phage dilution medium applied on sterile filter paper disk (**a** and **c**) or a 10 μL-droplet of sterile phage dilution medium (**b** and **d**); (**e**) upper left quadrant: 20 μL supernatant of ME1000 after extraction with chloroform and centrifugation; upper right quadrant: 20 μL ME1000; lower left quadrant: 20 μL of supernatant of MEPLC after extraction with chloroform and centrifugation; lower right quadrant: 10 μL of concentrated bacteriophage suspension. Figures f-k display results from antimicrobial activity assays of ISs prepared with ME1000, using the antimicrobial test of incorporation. Results from antibacterial activity of 500 μL **(f)** and 1000 μL **(g)** IS prepared with 0.3% (v/v) ME1000 upon a bacterial lawn of *P. aeruginosa*, of 500 μL **(h)** and 1000 μL **(i)** IS prepared with 0.6% (v/v) ME1000, and of 500 μL **(j)** and 1000 μL **(k)** IS prepared with 0.9% (v/v) ME1000. Inserted arrows pinpoint the lysis halos produced by encapsulated (i) or free (ii) phage particles.

lipid nanodroplets (Fig. 5c, MEPLC) to a more amorphous counterpart (Fig. 5e, ME1000), due to the imprisonment of the phage particles, thereby leading to the increased stability observed for ME1000. Regarding the thermogram of the concentrated PS (Fig. 5f), the two peaks appearing at 203.68 °C and 210.56 °C are most probably related to the lipid nature of the bacterial cell debris present in the suspension. Most notably, the thermogram produced for ME10 (Fig. 5d) exhibits only two main heat absorption events, one at 140.30 °C and another at 175.18 °C. Since this ME system was produced using a much smaller amount of phage particles (i.e., 100 times less than that offered in the preparation of ME1000), the absence of the third peak (present at ca. 191.22 °C in ME1000) was most likely related to the virtually nill amount of bacterial cell debris. Clearly, the widening of the melting profile range by a factor of 1.27 x ($\Delta T$ = 44.23 °C in ME1000; $\Delta T$ = 34.88 °C in ME10), implies a decreased crystallinity of ME1000 due to amorphization of the lipid envelope upon imprisonment of (one or more) phage particles.

### 3.8. Antibacterial activity of the W/O/W ME systems

The antibacterial activity of both ME10 and ME1000 was assessed *in vitro* against a pathogenic strain of *P. aeruginosa* (Fig. 6).

As can be seen from inspection of Fig. 6a–e, the concentrated PS demonstrated a very high lytic activity, as was expected (Fig. 6a–d, lower left quadrants). However, ME10 failed to exhibit any antibacterial activity (Fig. 6c and d, upper left quadrants). Several researchers reported no loss of phage viability with homogenization speeds up to 14,000 rpm [5]. But, after increasing the amount of phage virions offered by two orders of magnitude to $1.575 \times 10^9$ virions, the resulting ME1000 system displayed a pronounced antibacterial activity (Fig. 6a and b, upper left quadrants). MEPLC for ME10 and ME1000 were also produced and tested for antibacterial activity and, as expected, the results did not exhibit any antibacterial activity whatsoever (Fig. 6a–d, upper right quadrants). To test whether the dilution medium of the phage virions could somehow inhibit bacterial growth, a placebo suspension was also prepared by mixing LB-top agar (4 mL) and phage-buffer (3 mL), duly sterilized and tested in the same manner as the ME systems and the concentrated PS. As expected, the results did not exhibit any antibacterial activity whatsoever (Fig. 6a–d, lower right quadrants). Additionally, and since the phage virions in ME10 and ME1000 were extracted from the lipid nanodroplets with chloroform prior to testing for antibacterial activity, the antibacterial potential of ME1000 was compared when chloroform was used or not prior to plating. Fig. 6e displays in the upper left quadrant the result obtained for the ME1000 supernatant following extraction with chloroform and centrifugation, in the upper right quadrant the result obtained for plain ME1000, in the lower left quadrant the result obtained for the MEPLC supernatant after extraction with chloroform and centrifugation, and in the lower right quadrant the result obtained for the concentrated PS. As can be seen, extraction of phage particles from the lipid nanodroplets with chloroform did not exert any deleterious effect upon their lytic activity.

### 3.9. (Cryo-/NS-) TEM analyses

TEM analyses were performed with samples of concentrated PS and ME1000 via two different processes, viz. cryo-TEM and Negative-Staining TEM (NS-TEM). The structure of the lipid nanodroplets integrating the ME1000 system is shown in Fig. 7e and f, but the NS-TEM analysis was not able to distinguish phage particles within their inner aqueous core.

The process of coloration of particles with uranyl acetate involves a gentle air-drying of the sample following application of 3 μL of an aqueous solution of uranyl acetate at 2% (w/w) on the copper grid containing the sample. Although very gentle, such drying is sufficient to promote a deformation of the particles, and in fact this can be clearly observed in micrographs (**d**)–(**i**) in Fig. 7. On the contrary, TEM analyses following vitrification of the samples allows observation of particles as they really are, without any alterations in their shape, since the samples are vitrified with the particles suspended in a thin layer of amorphous ice. Notwithstanding this fact, TEM analyses following

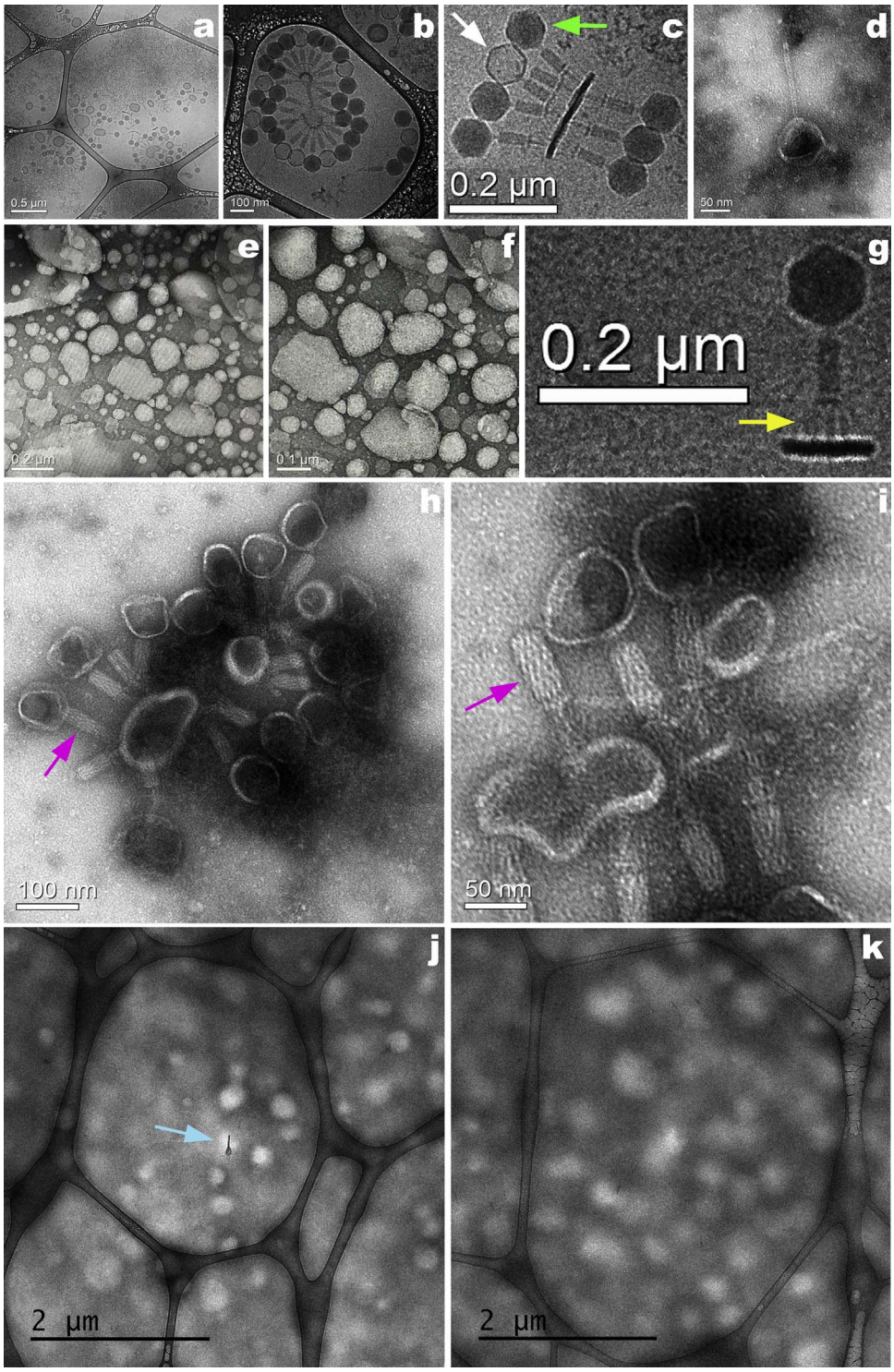


**Fig. 7.** Cryo-TEM micrographs of the concentrated PS, showing **(a)** the profusion of phage particles suspended in a layer of ice occupying several of the multitude of holes contained in the carbon grid used to prepare the sample just to show the representativeness of the analysis, **(b)** several phage particles attached to bacterial cell debris, **(c)** a detail of several phage particles attached to cell debris allowing to observe the tail fibers and the hexagonal capsids showing the presence (green arrow) and absence (white arrow) of dsDNA, **(g)** a single phage particle allowing to clearly observe the morphology of phage JG004 with its characteristic hexagonal capsid and tail fibers (yellow arrow); NS-TEM micrographs of **(d)** a phage particle, **(e)** and **(f)** ME1000, and (**h**) and (**i**) phage particles allowing to clearly observe the helical structure of its contractile sheath (pink arrows). Photomicrographs (**j**) and (**k**) were produced without any treatment of ME1000. (For interpretation of the references to colour in this figure legend, the reader is referred to the web version of this article.)

negative-staining of the samples allows observation of the particles with a greater contrast (e.g. micrographs (**d**)–(**h**) in Fig. 7). As voltage increases, so does the electron energy and, as a consequence, the electrons interact less with matter over a given thickness and therefore produce less contrast, which is a crytical parameter in cryo-TEM [49]. This was indeed the case with our analyses, since the TEM utilized for performing the analyses operated at 120 kV, an electron energy high enough to produce images with not so great contrast. Also, in Cryo-TEM analyses, particles are suspended in a layer of ice whose thickness may be much larger than the particles themselves, which further contributes to a poor contrast of the micrographs. This would more favorably be dealt with by a higher voltage, which produces a larger depth of field, however it would promote melting of the ice layer and damage the sample. Liquid ethane was used to vitrify our water-rich ME1000 samples for cryo-TEM, since a thin film of water quickly immersed in liquid ethane at −145 °C freezes too rapidly for water to crystallize and thus becomes amorphous. This rapid freezing by plunging the samples in liquid ethane does not disrupt the structure of both the phage particles and the soft aqueous-core lipid nanodroplets present in the liquid state, as the formation of ice crystals can do. Hence, cryo-TEM analyses allowed observation of particles in a near-native hydrated state since the samples were vitrified, keeping the particles suspended in a thin

layer of amorphous ice. Nevertheless, micrographs (**e**) and (**f**) allows to clearly observe the structure of the lipid nanodroplets integrating our ME1000 system, as well as the total absence of aggregation phenomena. Additionally, a careful inspection of TEM photomicrographs (**e**) e (**f**) allows to observe the existence of a dark line surrounding each particle. In fact, such line may correspond to an accumulation of the lipid surfactant (soybean lecithin) at the interface between lipid nanodroplets and the external aqueous phase of the ME system, translating into a higher concentration of carbon atoms at that same interface with concomitant higher opacity to penetration of electrons. Hence, the negative charge of the lipid surfactant that most likely accumulated at that interface may have contributed to the much negative ZP of the lipid nanodroplets housing phage particles in their inner aqueous core. In photomicrographs (**j**) and (**k**) in Fig. 7, produced with non-treated (pure) ME1000 samples, one can clearly observe the spherical shape of the lipid nanodroplets although the images are rather diffuse due to the thickness of the dried samples on the carbon grids. One can also observe a phage particle in photomicrograph (**j**) (light-blue arrow), and the higher density of carbon atoms in the phage particle (of protein nature) might allow to suggest that the particle was in fact encapsulated within the nanodroplet.

### 3.10. Determination of the cytotoxicity potential of the W/O/W ME systems, via the MTT assay

The MTT assays show cell viability found after exposure to increasing product concentrations (Fig. 8a), allowing to establish the half maximal inhibitory concentration ($IC_{50}$).

At the product concentrations tested in cells A549, both the concentrated PS and its placebo did not present a high toxicity, with these cells presenting a viability of ca. 80% with a product concentration around 10%. Regarding MEPLC, ME10 and ME1000, they all promoted a drop in cell viability ($IC_{50}$ values in Table 4).

From inspection of the data displayed in Table 4, one can observe that cells A549 presented a higher resistance to the treatments with the products, being necessary a higher concentration of product(s) to attain 50% of cell death. With cell line A549, treatment with products ME10 and ME1000 did not present significative differences, whereas with cell line V79 it was possible to verify a higher toxicity upon treatment with product ME1000 (Table 4 and Fig. 8a).

### 3.11. Determination of the apoptosis and necrosis potential of the W/O/W ME systems, via image cytometry (Tali® analysis)

The results obtained from the analysis of cell death type were gathered using 10% of the concentration of the original products (Fig. 9a). Although cells A549 presented a $IC_{50}$ higher than that of cells V79, when they were evaluated with a concentration at 10% of the original products they presented a low index of viability, with the majority of the cells dying from necrosis (Fig. 9a), except for the treatment with product ME1000, which promoted cell death by apoptosis in a larger proportion. The treatments performed with cell line V79 promoted a lower index of cell death, with the majority of cell deaths occurring by apoptosis.

From the results displayed in Fig. 9a, one may conclude that the products studied present a low cytoxicity when in concentrations below 10% of the original (stock) products, with the different cell lines appearing to respond in a differentiated manner to the treatments. It must also be considered that although the concentrated PS did not present any toxicity, proving that its utilization is safe, and that the nanoencapsulation procedure resulted in a product (ME1000) that seems to promote cell suffering during the first 24 h, it is necessary to verify if cellular stability is recovered after this initial period of time through new analyses of viability *vs*. time. The results from these analyses show that cells treated with the products exhibited a lower cell viability, presenting a total of cells less than that of the negative control. The cells treated with the tested products presented a high index of apoptosis and necrosis, which can be found mainly in the relative data displayed in Fig. 9a. The results show that MEPLC, ME10 and ME1000 have an effect on cell viability, being possible to use them in concentrations below 4% (ME10) or 1% (ME1000), as these were the $IC_{50}$ concentrations for each sample tested.

### 3.12. Antibacterial potential of the ISs integrating the ME1000 system

Due to the very low amounts of ME1000 added to the saline solution, the resulting mixtures were naturally already isotonic and suitable for administration via nebulization. The results obtained for the antibacterial properties of these ISs, formulated with ME1000, are displayed in Fig. 6f–k for different volume concentrations, viz. 0.3% (v/v) (**f** (500 μL) and **g** (1000 μL)), 0.6% (v/v) (**h** (500 μL) and **i** (1000 μL)), and 0.9% (v/v) (**j** (500 μL) and **k** (1000 μL)). From inspection of Fig. 6f–k (inserted arrows), different patterns of lysis were produced when phage particles were encapsulated (i) or remained in free form (ii) in ME1000. Since the volume usually projected during a nebulization jet is of the order of magnitude of 500 μL, and because (at least in theory) a single phage particle would be sufficient to completely eradicate a bacterial infection, all the ISs tested would be highly effective in eradicating a lung bacterial infection by *P. aeruginosa*.

### 3.13. Determination of the cytotoxicity potential of the ISs integrating the ME1000 system, via the MTT assay

The cellular viability data obtained upon exposure of the three cell lines to the ISs prepared with ME1000 is displayed in Fig. 8b. When testing the viability of concentrated ME1000, one noticed that concentrations between 0.3% to 0.9% (v/v) exhibited a good cell viability for the different cell lines, and so new saline solutions were prepared at concentrations of 0.3%, 0.6% and 0.9% (v/v) so as to be tested regarding their effects upon cell viability, either via MTT analyses or image cytometry. For the MTT analyses, the (isotonic) saline solutions were further diluted to 35%, 30%, 25%, 20%, 15%, 10%, 5% and 1% (v/v) and, for the cell viability, necrosis and apoptosis the saline solutions were always tested at a concentration of 30% (v/v). The results obtained (Fig. 8b) show that, at this concentration, the different cell lines did not present cell death higher than 50%, with the cell type most sensitive being V79 which, at a concentration of 35% (v/v) of the ISs, displayed 50% of cell death.

### 3.14. Determination of the apoptosis and necrosis potential of the ISs integrating the ME1000 system, via image cytometry (Tali® analysis)

The results gathered via image cytometry (Fig. 9b) clearly show that, when tested at 30% (v/v) of the different concentrations of the isotonic saline solutions, the cells exhibited a high viability. It is possible to observe that the major part of cell death in line V79 occurs due to necrosis and not due to induction by cell apoptosis, and in cell lines 3T3 and A549 it is possible to observe an equilibrium between the two types of cell death (Fig. 9b). Based on the results obtained pertaining to cell viability tests (both MTT and image cytometry), it is possible to argue that the ISs tested exhibited a good cell viability, while displaying a low cell toxicity.

### 3.15. Determination of the oxidative stress potential of the ISs integrating the ME1000 system

The possible oxidative stress effects of the ISs prepared with ME1000 are displayed in Fig. 10 for the three cell lines evaluated, in the form of relative stress indexes.

The oxidative stress tests revealed that cell treatments with all ISs resulted in cell stress levels significantly higher than that of the positive control (Two-Way ANOVA at 5% significance, with those results

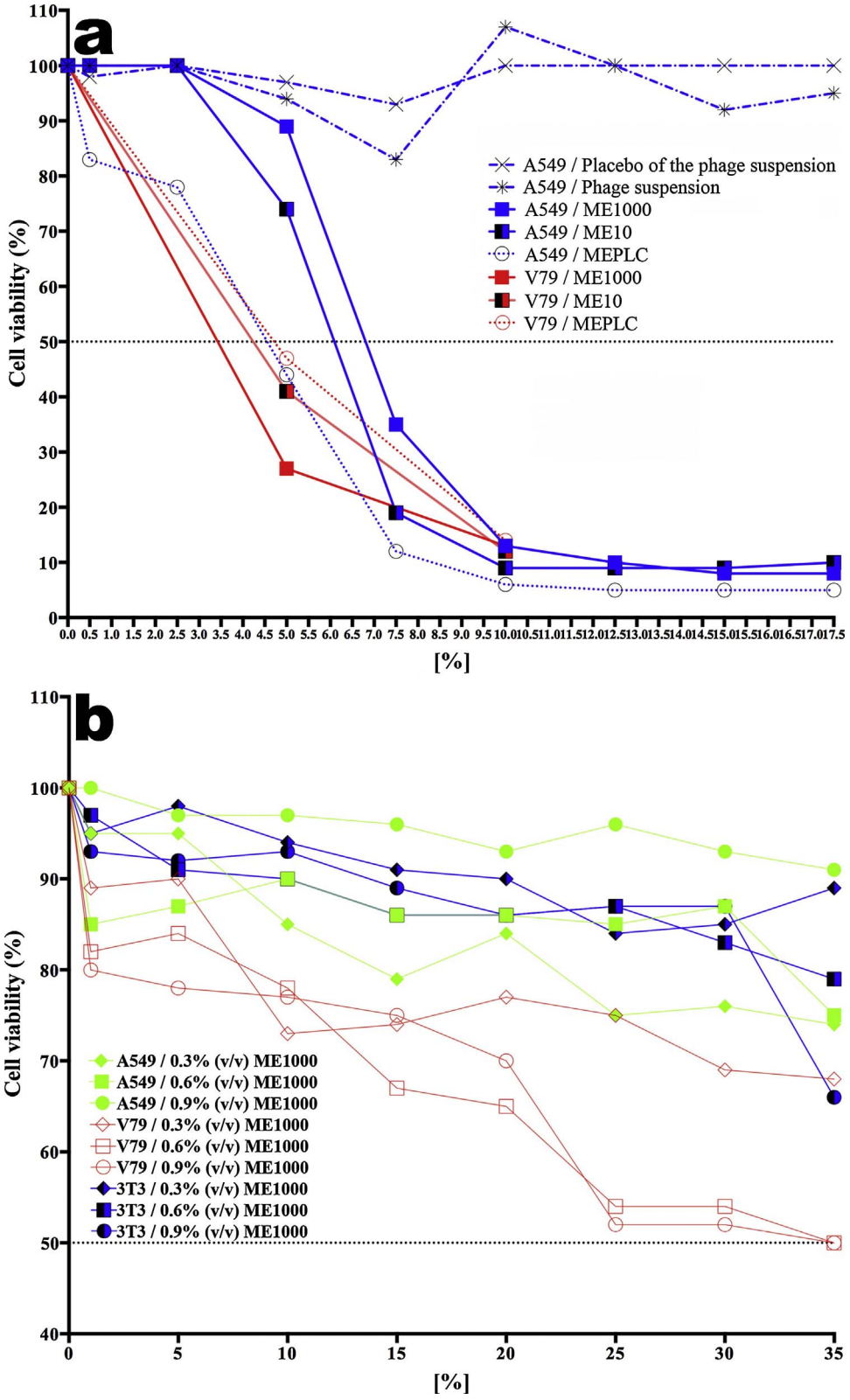


**Fig. 8.** Results from cellular viability (MTT assays) (**a**) using cell lines A549 and V79 cultured in DMEM medium to evaluate the cytotoxicity of placebo of PS, concentrated PS, MEPLC, ME10 and ME1000, during a 24 h treatment period at different concentrations, and (**b**) using cell lines V79, 3T3 and A549 cultured in DMEM medium to evaluate the cytotoxicity of ISs prepared with ME1000, during a 24 h treatment period at different concentrations (means (n = 5), with $\sigma < 0.1$).

statistically different from that of the control marked with '*'), existing a slight variation among cell lines (Fig. 10). In general, an increase in the oxidative stress reflects in higher cell apoptosis, which is possible to verify when comparing the results obtained in the oxidative stress analyses with the results from apoptosis/necrosis, allowing to clearly observe an increase in the apoptosis of the cell line V79, mainly with the IS at a concentration of 0.3% (v/v) (Fig. 10).

### *3.16. Determination of the DNA damage potential of the ISs integrating the ME1000 system, via comet™ assay*

To evaluate any possible genetic damage to the cells imparted by the saline ISs integrating ME1000, the Comet™ test was carried out with lung cell lines (V79 and A549), allowing to observe no significant differences between the control and the lung cell lines that were exposed to the ISs (Fig. 11).

**Table 4**
Results obtained for the IC50 values via MTT assays with cell lines A549 and V79, exposed to the concentrated bacteriophage suspension, to the placebo of the phage suspension, and to W/O/W multiple emulsion systems MEPLC, ME10 and ME1000.

| Cell line | Product used in treatment | $IC_{50}$ |
|---|---|---|
| A549 | Concentrated bacteriophage suspension | Not cytotoxic up to 17.5% |
| | Placebo of the bacteriophage suspension | Not cytotoxic up to 17.5% |
| | MEPLC | 4.55% |
| | ME10 | 6.11% |
| | ME1000 | 6.87% |
| V79 | MEPLC | 4.76% |
| | ME10 | 4.23% |
| | ME1000 | 3.38% |

This means that the ISs tested do not possess characteristics that promote lesions in the DNA. If one compares these results with the results generated by both the oxidative stress analyses and apoptosis/necrosis, it is possible to observe that lung cell lines V79 and A549 did not exhibit a high apoptosis index, although signaling an increase in the oxidative stress relative to that of the control. Fig. 11 represents the genotoxic effects (DNA damage index) of lung cell lines V79 and A549 incubated with ISs integrating variable amounts of ME1000. For A549 and V79 cell lines, the ISs integrating ME1000 showed no significant genotoxic effects at the three tested concentrations (viz., 0.3%, 0.6% and 0.9%, v/v). These results are in clear agreement with the lack of cytotoxic effects observed for both cell lines (Fig. 8b). Hence, the lack of cytotoxic effects is in line with the lack of DNA damage, which is in clear agreement with results published elsewhere [42].

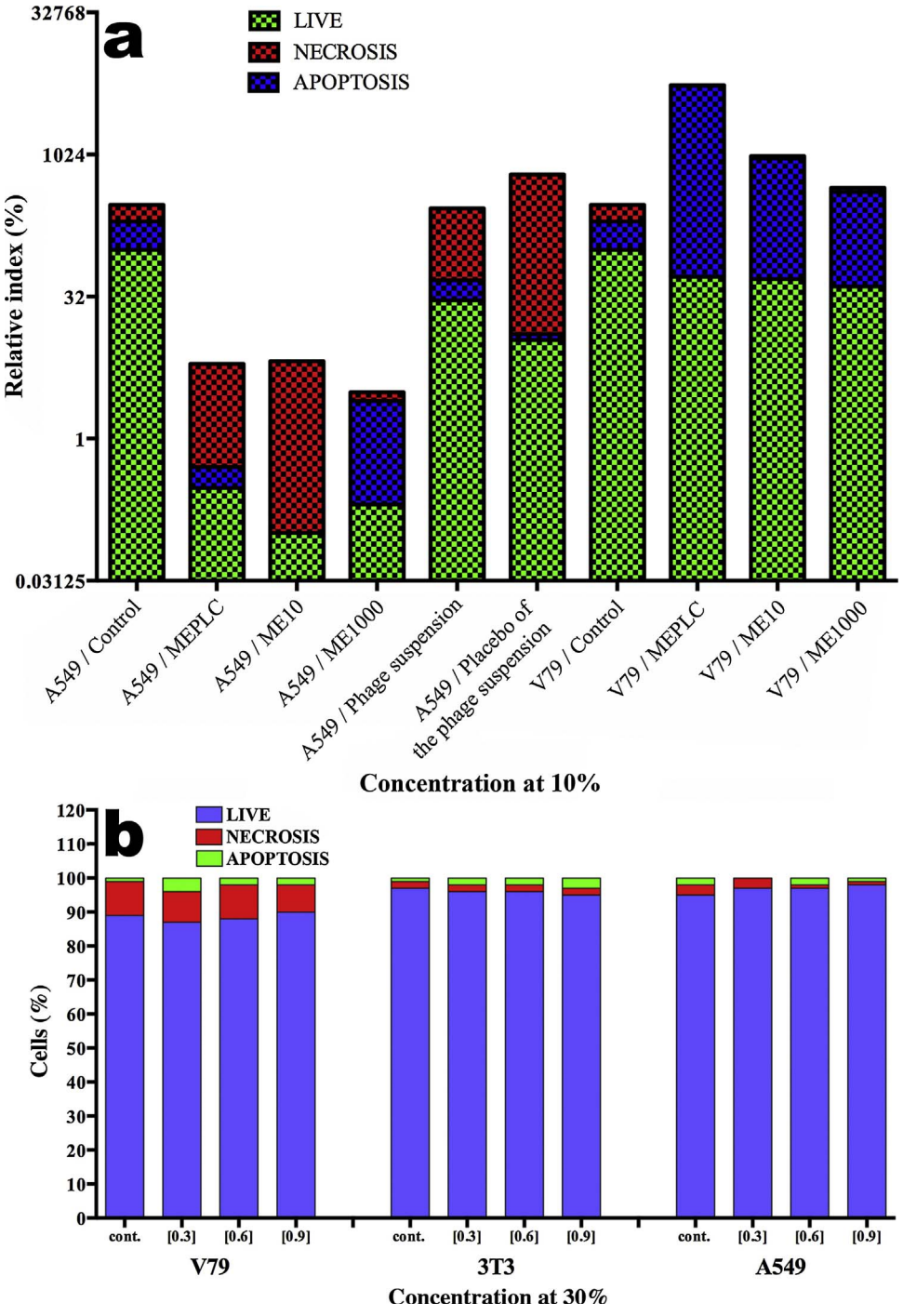


**Fig. 9.** Relative indexes of cell necrosis and apoptosis in (**a**) cell lines A549 and V79 following treatment with the placebo of PS, the concentrated PS, MEPLC, ME10 and ME1000, with concentrations set at 10% of the initial values, and in (**b**) cell lines V79, 3T3 and A549, following treatment with the ISs prepared with ME1000, with concentrations set at 30% of the initial values (means (n = 5), with $\sigma < 0.1$).

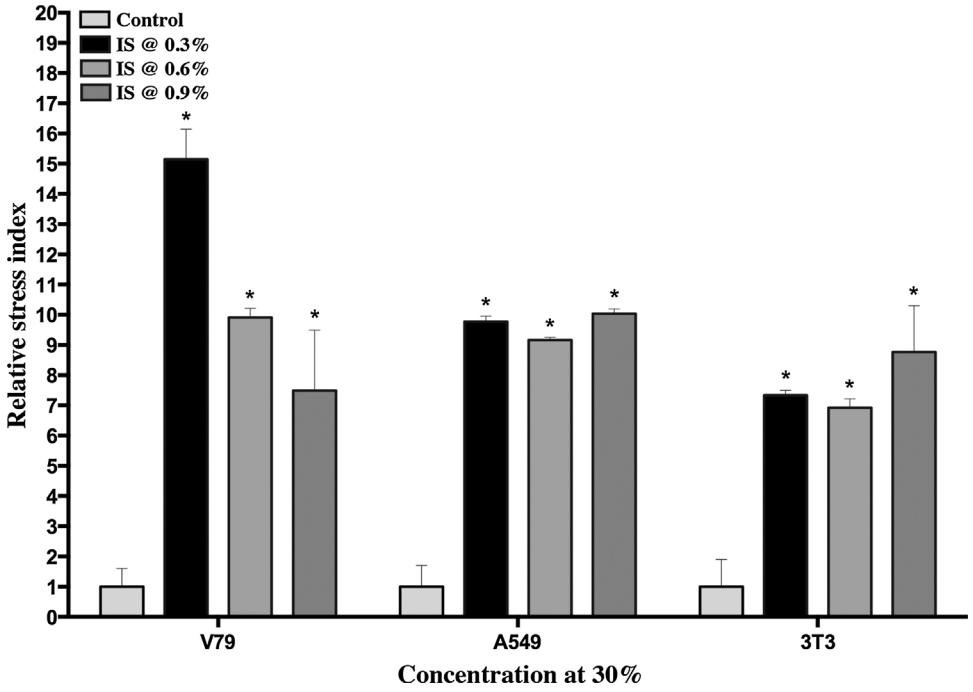


**Fig. 10.** Relative stress indexes of cell lines V79, 3T3 and A549 following oxidative stress induced by treatment with the ISs prepared with ME1000 at 0.3%, 0.6% and 0.9% (v/v), with concentrations set at 30% of the initial values. Means of five experiments (n = 5; Two-Way ANOVA at 5% significance), with results statistically different from those of the control marked with '*', with associated σ: **V79** (control, 1.000 ± 0.600; IS@0.3%, 15.147 ± 1.000; IS@0.6%, 9.912 ± 0.300; IS@0.9%, 7.492 ± 2.000), **A549** (control, 1.000 ± 0.700; IS@0.3%, 9.768 ± 0.190; IS@0.6%, 9.168 ± 0.090; IS@0.9%, 10.035 ± 0.160), **3T3** (control, 1.000 ± 0.900; IS@0.3%, 7.340 ± 0.160; IS@0.6%, 6.920 ± 0.300; IS@0.9%, 8.765 ± 1.540).

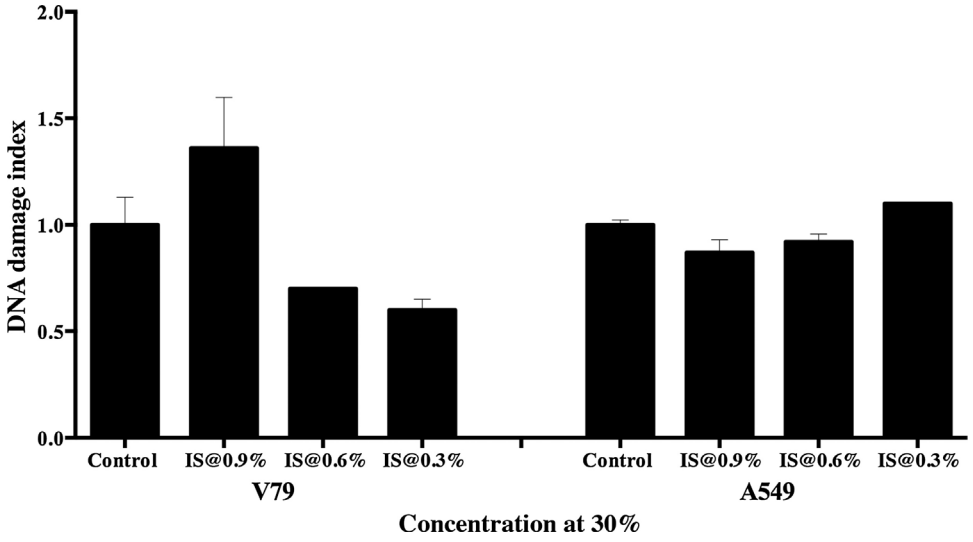


**Fig. 11.** DNA damage indexes of lung cell lines V79 and A549 following exposure to the ISs prepared with ME1000 at 0.3%, 0.6% and 0.9% (v/v), with concentrations set at 30% of the initial values. Means of three experiments with associated σ: **V79** (control, 1.000 ± 0.130; IS@0.3%, 0.600 ± 0.050; IS@0.6%, 0.700 ± 0.000; IS@0.9%, 1.360 ± 0.238), **A549** (control, 1.000 ± 0.023; IS@0.3%, 1.100 ± 0.000; IS@0.6%, 0.920 ± 0.036; IS@0.9%, 0.870 ± 0.060).

## 4. Conclusions

Imprisonment of phage particles in a nano-sized aqueous core promotes a change in the thermodynamic conditions of the nanoenvironment surrounding each phage particle due to the fact that the movements of (aqueous) solvent molecules in their microneighborhood become seriously reduced by the effect of being contained within the matrix's aqueous core, thereby leading to enhanced thermodynamic stability. The net result is a potentiation of the phage particle's rotational, translational and vibrational viscosity, promoting a more rigid three-dimensional architecture of the particle with concomitant decrease of entropy and thus promoting its structural and functional stabilization [3,4,8–10,32]. For A549 and V79 cell lines, the three ISs integrating ME1000 showed no significant genotoxic effects, which was in clear agreement with the lack of cytotoxic effects observed for both cell lines. The use of ME1000 in formulating an IS for nebulization in the treatment of bacterial (*P. aeruginosa*) lung infections, would possess inherent advantages, when compared with the current chemical antibiotherapy, in that specific and strictly lytic phages are natural self-replicating predators of bacteria that continuously replicate at the site of infection while there are still viable host cells, while being virtually harmless to human cells and tissues.

## Acknowledgements

Project funding by FAPESP (São Paulo, Brazil; Refs. No. **2013/03181-6 (Project PneumoPhageKill), 2016/08884-3 (Project PneumoPhageColor) and 2016/12234-4 (Project TransAppIL))**, is hereby gratefully acknowledged. This work also received support from CNPq, in the form of a Research Productivity (PQ) fellowship granted to Victor M. Balcão (**Ref. No. 306113/2014-7**). The authors are grateful to the LME facility at LNNano/CNPEM (Campinas, Brazil) for the use of the TEM microscope. The authors have no conflicts of interest whatsoever to declare.

## References

[1] B.K. Chan, S.T. Abedon, C. Loc-Carrillo, Phage cocktails and the future of phage

therapy, Future Microbiol. 8 (6) (2013) 769–783.
[2] I.U. Haq, W.N. Chaudhry, M.N. Akhtar, S. Andleeb, I. Qadri, Bacteriophages and their implications on future biotechnology: a review, Virol. J. 9 (2012) 2–8.
[3] V.M. Balcão, A.R. Moreira, C.G. Moutinho, M.V. Chaud, M. Tubino, M.M.D.C. Vila, Structural and functional stabilization of phage particles in carbohydrate matrices for bacterial biosensing, Enzyme Microb. Technol. 53 (1) (2013) 55–69.
[4] V.M. Balcão, S.V.P. Barreira, T.M. Nunes, M.V. Chaud, M. Tubino, M.M.D.C. Vila, Carbohydrate hydrogels with stabilized phage particles for bacterial biosensing: bacterium diffusion studies, Appl. Biochem. Biotechnol. 172 (3) (2014) 1194–1214.
[5] U. Puapermpoonsiri, J. Spencer, C.F. van der Walle, A freeze-dried formulation of bacteriophage encapsulated in biodegradable microspheres, Eur. J. Pharm. Biopharm. 72 (1) (2009) 26–33.
[6] A. Sulakvelidze, E. Kutter, Bacteriophage therapy in humans, in: E. Kutter, A. Sulakvelidze (Eds.), Bacteriophages: Biology and Applications, CRC Press, 2005, pp. 381–436.
[7] A. Sulakvelidze, Z. Alavidze, J.G. Morris Jr., Bacteriophage therapy, Antimicrob. Agents Chemother. 45 (3) (2001) 649–659.
[8] C.A. Glasser, M.M.D.C. Vila, J.C. Pereira, M.V. Chaud, J.M. Oliveira Júnior, M. Tubino, V.M. Balcão, Development of a water-in-oil-in-water multiple emulsion system integrating biomimetic aqueous-core lipid nanodroplets for protein entity stabilization. Part II: process and product characterization, Drug Dev. Ind. Pharm. 42 (12) (2016) 1990–2000.
[9] V.M. Balcão, M.M.D.C. Vila, Structural and functional stabilization of protein entities: state-of-the-art, Adv. Drug Deliv. Rev. 93 (2015) 25–41.
[10] V.M. Balcão, C.I. Costa, C.M. Matos, C.G. Moutinho, M. Amorim, M.E. Pintado, A.P. Gomes, M.M. Vila, J.A. Teixeira, Nanoencapsulation of bovine lactoferrin for food and biopharmaceutical applications, Food Hydrocoll. 32 (2) (2013) 425–431.
[11] P.R. Srinivas, M. Philbert, T.Q. Vu, Q. Huang, J.L. Kokini, E. Saos, H. Chen, C.M. Peterson, K.E. Friedl, C. McDade-Ngutter, V. Hubbard, P. Starke-Reed, N. Miller, J.M. Betz, J. Dwyer, J. Milner, S.A. Ross, Nanotechnology research: applications in nutritional sciences, J. Nutr. 140 (2010) 119–124.
[12] M. Gallarate, M. Trotta, L. Battaglia, D. Chirio, Preparation of solid lipid nanoparticles from w/o/w emulsions: preliminary studies on insulin encapsulation, J. Microencapsul. 26 (2009) 394–402.
[13] S. Yang, W. Yuan, T. Jin, Formulating protein therapeutics into particulate forms, Expert Opin. Drug Deliv. 6 (2009) 1123–1133.
[14] M. Rawat, D. Singh, S. Saraf, S. Saraf, Lipid carriers: a versatile delivery vehicle for proteins and peptides, Yakugaku Zasshi (The Pharmaceutical Society of Japan) 128 (2008) 269–280.
[15] S.A. Wissing, O. Kayser, R.H. Müller, Solid lipid nanoparticles for parenteral drug delivery, Adv. Drug Deliv. Rev. 56 (2004) 1257–1272.
[16] J.F. Fangueiro, T. Andreani, M.A. Egea, M.L. Garcia, S.B. Souto, E.B. Souto, Experimental factorial design applied to mucoadhesive lipid nanoparticles via multiple emulsion process, Colloids Surf. B: Biointerfaces 100 (2012) 84–89.
[17] D. Dupeyrón, J. Rieumont, M. González, V.M. Castaño, Protein delivery by enteric copolymer nanoparticles, J. Dispers. Sci. Technol. 30 (2009) 1188–1194.
[18] J.A. Hanson, C.B. Chang, S.M. Graves, Z. Li, T.G. Mason, T.J. Deming, Nanoscale double emulsions stabilized by single-component block copolypeptides, Nature 455 (2008) 85–88.
[19] Y.F. Wang, Z. Tao, H. Gang, Structural evolution of polymer-stabilized double emulsions, Langmuir 22 (2006) 67–73.
[20] M. García-Fuentes, D. Torres, M.J. Alonso, Design of lipid nanoparticles for the oral delivery of hydrophilic macromolecules, Colloids Surf. B: Biointerfaces 27 (2003) 159–168.
[21] J. Bibette, F.L. Calderon, P. Poulin, Emulsions: basic principles, Rep. Prog. Phys. 62 (1999) 969–1033.
[22] M.F. Ficheux, L. Bonakdar, F. Leal-Calderon, J. Bibette, Some stability criteria for double emulsions, Langmuir 14 (1998) 2702–2706.
[23] J. Araújo, E. Gonzalez, M.A. Egea, M.L. Garcia, E.B. Souto, Nanomedicines for ocular NSAIDs: safety on drug delivery, Nanomedicine 5 (2009) 394–401.
[24] J. Araújo, E. Vega, C. Lopes, M.A. Egea, M.L. Garcia, E.B. Souto, Effect of polymer viscosity on physicochemical properties and ocular tolerance of FB-loaded PLGA nanospheres, Colloids Surf. B: Biointerfaces 72 (2009) 48–56.
[25] A. Nakou, M. Woodhead, A. Torres, MRSA as a cause of community-aquired pneumonia, Eur. Respir. J. 34 (5) (2009) 1013–1014.
[26] A. El Solh, A.A. Alhajhusain, Update on the treatment of *Pseudomonas* pneumonia, J. Antimicrob. Chemother. 64 (2009) 229–238.
[27] R.N.T. Turrini, A.H. Santo, Infecção hospitalar e causas múltiplas de morte [Hospital-acquired infection and multiple causes of death], J. Pediatr. (Rio. J) 78 (6) (2002) 485–490.
[28] P. Davey, E. Brown, L. Fenelon, R. Finch, I. Gould, A. Holmes, C. Ramsay, E. Taylor, P. Wiffen, M. Wilcox, Systematic review of antimicrobial drug prescribing in hospitals, Emerg. Infect. Dis. 12 (2) (2006) 211–216.
[29] G.H.C. Furtado, M.D. Bergamasco, F.G. Menezes, D. Marques, A. Silva, L.B. Perdiz, S.B. Wey, E.A.S. Medeiros, Imipenem-resistant *Pseudomonas aeruginosa* infection at a medical-surgical intensive care unit: risk factors and mortality, J. Crit. Care 24 (2009) 625. e9-625. e14.
[30] L.N.S. Alves, C.R. Oliveira, L.A.P. Silva, S.M.D. Gervásio, S.R. Alves, G.M. Sgavioli, Hemoculturas: estudo da prevalência dos microrganismos e o perfil de sensibilidade dos antibióticos utilizados em Unidade de Terapia Intensiva [Hemocultures: a study of the prevalence of microorganisms and the sensitivity profile of the antibiotics used in the Intensive Care Unit], J. Health Sci. Inst. 30 (1) (2012) 44–47.
[31] C.A. Glasser, M.M.D.C. Vila, J.C. Pereira, M.V. Chaud, J.M. Oliveira Júnior, M. Tubino, V.M. Balcão, Development of a water-in-oil-in-water multiple emulsion system integrating biomimetic aqueous-core lipid nanodroplets for protein entity stabilization: part I: experimental factorial design, Eur. J. Biomed. Pharm. Sci. 3 (3) (2016) 65–74.
[32] V.M. Balcão, C.A. Glasser, M.V. Chaud, F.S. V.del Fiol, M. Tubino, M.M.D.C. Vila, Biomimetic aqueous-core lipid nanodroplets integrating a multiple emulsion formulation: a suitable housing system for viable lytic bacteriophages, Colloids Surf. B: Biointerfaces 123 (2014) 478–485.
[33] B.I. Erdinc, Micro/Nanoencapsulation of Proteins Within Alginate/Chitosan Matrix by Spray Drying, M.Sc Thesis, Queen's University, Kingston, Ontario, Canada, 2007 pp. 90.
[34] V. Ragoonanan, A. Aksan, Protein stabilization, Transfus. Med. Hemotherapy 34 (2007) 246–252.
[35] M.L. Ferrer, L. Yuste, F. Rojo, F. del Monte, Biocompatible sol-gel route for encapsulation of living bacteria in organically modified silica matrixes, Chem. Mater. 15 (2003) 3614–3618.
[36] M.R. Mozafari, K. Khosravi-Darani, G.G. Borazan, J. Cui, A. Pardakhty, S. Yurdugul, Encapsulation of food ingredients using nanoliposome technology, Int. J. Food Properties 11 (2008) 833–844.
[37] P. Severino, T. Andreani, A.S. Macedo, Fangueiro, M.H.A.J.F. Santana, A.M. Silva, E.B. Souto, Current state of-art and new trends on lipid nanoparticles (SLN and NLC) for oral drug delivery, J. Drug Deliv. 2012 (2012) 10, http://dx.doi.org/10.1155/2012/750891 Article ID 750891.
[38] E.B. Souto, V. Teeranachaideekul, P. Boonme, R.H. Muller, V.B. Junyapraset, Lipid-based nanocarriers for cutaneous administration of pharmaceutics, Encyc. Nanosci. Nanotechnol. 15 (2011) 479–491.
[39] B. Heike, Structural properties of solid lipid based colloidal drug delivery systems, Curr. Opin. Colloid Interface Sci. 16 (2011) 405–411.
[40] T. Schmidts, D. Dobler, C. Nissing, F. Runkel, Influence of hydrophilic surfactants on the properties of multiple W/O/W emulsions, J. Colloid Interface Sci. 338 (1) (2009) 184–192.
[41] M.E. Carlotti, M. Gallarate, S. Sapino, E. Ugazio, W/O/W multiple emulsions for dermatological and cosmetic use, obtained with ethylene oxide free emulsifiers, J. Dispers. Sci. Technol. 26 (2005) 183–192.
[42] A.B. Seabra, T. Pasquôto, A.C. Ferrarini, M.C. Santos, P.S. Haddad, R. Lima, Preparation, characterization, cytotoxicity, and genotoxicity evaluations of thiolated- and s-nitrosated superparamagnetic iron oxide nanoparticles: implications for cancer treatment, Chem. Res. Toxicol. 27 (7) (2014) 1207–1218.
[43] A.G. Oliveira, M.V. Scarpa, M.A. Correa, L.F.R. Cera, T.P. Formariz, Microemulsions: structure and application as drug delivery systems, Quím. Nova 27 (1) (2004) 131–138.
[44] A.R. Pianovski, A.F.G. Vilela, C.G. Lima, K.K. Silva, V.F.M. Carvalho, C.R. De Musis, S.R.P. Machado, M. Ferrari, Development and evaluation of O/W/O multiple emulsions stability containing pequi oil (*Caryocar brasiliense*), Rev. Bras. Farm. 89 (2) (2008) 155–159.
[45] N. Schultz, G. Metreveli, M. Franzreb, F.H. Frimmel, C. Syldatk, Zeta potential measurement as a diagnostic tool in enzyme immobilisation, Colloids Surf. B Biointerfaces 66 (1) (2008) 39–44.
[46] J. Jiao, D. Burgess, Rheology and stability of water-in-oil-in-water multiple emulsions containing Span 83 and Tween 80, AAPS PharmSci. 5 (2003) 1–12.
[47] H. Bunjes, T. Unruh, Characterization of lipid nanoparticles by differential scanning calorimetry, X-ray and neutron scattering, Adv. Drug Deliv. Rev. 59 (2007) 379–402.
[48] K. Katayama, H. Nomura, H. Ogata, T. Eitoku, Diffusion coefficients for nanoparticles under flow and stop-flow conditions, Phys. Chem. Chem. Phys. 11 (2009) 10494–10499.
[49] A. des Georges, Y. Hashem, S.N. Buss, F. Jossinet, Q. Zhang, H.Y. Liao, J. Fu, A. Jobe, R.A.R. Grassucci Langlois, C. Bajaj, E. Westhof, S. Madison-Antenucci, J. Frank, High-resolution cryo-EM structure of the *Trypanosoma brucei* Ribosome: a case study, in: T. Gabor Herman, Joachim Frank (Eds.), Computational Methods for Three-Dimensional Microscopy Reconstruction, Birkhäuser, 978-1-4614-9520-8, 2014, pp. 97–132 Chapter 5.